Joint Centre for Mesoscale Meteorology, Reading, UK

Observations and Model Simulations of the FAXTEX IOP 16 Frontal Wave-Effects of Sublimation

S. A. Clough
H. W. Lean
N. M. Roberts
R. M. Forbes

Internal Report No. 98

December 1998

Met Office Joint Centre for Mesoscale Meteorology Department of Meteorology
University of Reading PO Box 243 Reading RG6 6BB United Kingdom
Tel: +44 (0)118 931 8425 Fax: +44 (0)118 931 8791
www.metoffice.com

Designed and produced by the Met Office © Crown copyright 2001 01/0240 The Met Office logo is a registered trademark.

Observations and Model Simulations of the FASTEX IOP 16 Frontal Wave - Effects of Sublimation.

by

Sid A Clough, Humphrey W Lean, Nigel M Roberts and Richard M Forbes

16 December 1998

(Submitted to the Quarterly Journal of the Royal Meteorological Society, December 1998)

Abstract

The dynamical role of sublimation in weather systems is briefly reviewed. Observations are presented from FASTEX IOP 16 that show variations of static stability, humidity and mesoscale circulation corresponding to those associated theoretically with sublimation of ice precipitation. It is thus suggested that the observations display the mechanism proposed by Clough and Franks in which forward mesoscale flows are associated with moist adiabatic descent supported by the sublimation cooling. This mechanism was suggested as an important stage in the evolution of many mesoscale rainbands.

A set of 3 model simulations of the event has been made with versions of the Meteorological Office's Unified Model. Of these a mesoscale model integration with 11 km resolution and 45 levels clearly displays the symptoms and is diagnosed to demonstrate its consistency with the Clough-Franks mechanism. An integration with omission of the cooling due to sublimation differs significantly from the full model experiment in the structure of low level

wind fields, frontal troughs and mesoscale precipitation distribution. It is also demonstrated that the stability transition and mesoscale circulation are substantially weakened in this integration, thus confirming that the hypothesised mechanism is also operating in the NWP model.

We deduce from these studies that ice precipitation and its sublimation has a major role in determining mesoscale circulation and structure in mid-latitude weather systems, affecting stratification and the formation of features such as fronts and rainbands. These are substantially affected by the fall and evaporation of ice crystals, which are both important to temperature and moisture transports and the behaviour of NWP models on time scales of hours to days. In our integrations dynamical feedback due to sublimation was associated with the extreme negative potential vorticity values predicted by the model, and hence the anticyclonic motion occurring in the cloud head or deep cloud of the moist warm sector as in this case. In this latter situation a substantial role for sublimation may be anticipated more generally.

We suggest that the described phenomenon be referred to as sublimation enhanced descent (SED).

It is concluded that in view of this demonstrated sensitivity substantial attention should be given to refining microphysical parametrisations in NWP models, and that observations from the FASTEX experiment provide a suitable basis for validating these schemes.

Section 1

Introduction

The study of cloud processes, forecasting and weather system dynamics have long been regarded as distinct specialisations within meteorology. Such distinctions do not exist in the atmosphere, and the ascendancy of numerical modelling is forcing us to transcend them. Two particular examples are important in the present context.

Firstly, most of the structural features evident in satellite imagery from active weather systems are produced by the formation and dissipation of ice clouds. Yet these are commonly interpreted in forecasting or dynamical terms with no reference to the properties of ice crystals and the microphysics of their formation or fate. Secondly, theories of the development of mesoscale rainbands developed from dynamical ideas that required only latent heat release regardless of details of cloud and precipitation microphysical processes.

Modern NWP models, however, contain complex parametrisations describing putative cloud microphysical and dynamical properties. It is essential to future progress that these models be interpreted within a physical framework which embraces the basic physics of the atmospheric processes represented. This is the central purpose of the present work.

Suppose we consider the cloud and precipitation processes as a hierarchy ordered by their importance in the latent heating budget of a system. Then the

leading term, release of latent heat on ascent, is indeed positive and independent of microphysics (to the extent that the modifying effect of glaciation is ignored). This is part of the reason why NWP has for so long been able to forecast large scale precipitation with little attention to microphysics. The other part is that the microphysical processes of ice are actually so fast that they permit highly efficient ice crystal growth by diffusion; the dynamics of vapour supply is the rate limiting step (Wexler and Atlas, 1958). Physically this is evident in that most of the time weather system precipitation is crystalline rather than heavily rimed, because crystal growth is able to keep pace with moisture supply at mesoscale ascent rates of around 30 cms^{-1} or less.

The next most important term in mid-latitudes is the cooling of the atmosphere in sublimation of ice precipitation, which can in principle exceed the latent heat release locally. Unlike the latent heat release term, however, the sublimation rate is highly sensitive to both particle characteristics and ambient conditions. Sublimation is also very fast, since diffusion growth of crystals is almost reversible at microscopic scales; commonly particle 1/e-folding times for sublimation are of order 10 minutes. However, because ice crystals interact so strongly with their environment the availability of precipitation and variation of thermodynamic state in the fall path become critical.

The complex and interesting behaviour of sublimation has received very little attention in the literature. Two paradigms have been suggested.

In the first, Harris (1977) attempted to explain downdrafts of several metres per second in Doppler radar observations by sublimation into the sub-cloud layer.

He successfully used microphysical model calculations to show that the layer immediately beneath cirrus cloud can be cooled so intensely that static instability may eventually result and hence lead to dry convection.

A second situation was envisaged by Clough and Franks (1991; hereafter referred to as CF), who suggested that the detailed physics of sublimation is likely to play an important role in the occurrence and structure of broad (10-100's km) rainbands (or snowbands). From simple kinetic-thermodynamic models they showed that in stable conditions sublimation should be capable of maintaining moist slantwise descending mesoscale circulations of up to 20-30 cms^{-1} in ice precipitation, typical of those occurring in many rainbands. Such moist slantwise descent they argued was an essential requirement to the occurrence of spatially extensive multiple bands via conditional symmetric instability (Bennetts and Hoskins, 1979) or a similar mechanism.

These two scenarios are quite different, in some respects complementary, and may both co-exist within a weather system. The latter, however, has a clear implication for mesoscale weather system dynamics. The prediction of slantwise descent has been confirmed qualitatively by Marecal and Lemaitre (1995) in Doppler radar observations and model calculations showing the importance of subliming snow in the mesoscale descent zone of an observed rainband.

The Fronts and Atlantic Storm Tracks Experiment (FASTEX) presents the ideal opportunity to pursue this problem quantitatively by providing collocated dropsonde, Doppler radar and aircraft microphysical observations capable of

validating mesoscale model predictions (Joly et al, 1997). During January and February 1997 this combination of observing platforms was used to characterise mesoscale weather system structure of several mid-latitude frontal systems in unprecedented detail. In a number of Intensive Observing Periods (IOPs) aircraft equipped with Doppler radar and dropsondes flew together along adjacent parallel tracks so that both clear and precipitating cloudy regions were observed over distances of 400-800 km, removing many of the limitations of coverage normally encountered in weather system study.

Of the events observed IOP 16 is best suited to the present study because of the simplicity of both the weather system and flight pattern. A rapidly moving trough intensified to form a low pressure centre in the period of the aircraft dropsonde and radar observations. The aircraft flew a simple set of 6 equally spaced tracks nearly perpendicular to the system track. This pattern permits model validation in unique detail and ultimately should permit comparison with microphysical process rates systematically calculated from the complementary observational datasets.

In this study we draw attention to a number of observed features of IOP 16, which we take to be symptomatic of sublimation and the associated slantwise descent. As well as thermodynamic structure these include dynamical effects indicating mesoscale circulations driven by the cooling, according to the mechanism of CF. A number of mesoscale model simulations of the event are then presented in which comparable features are indicated and the role of sublimation is demonstrated. It is argued that this role primarily is to modify the effective static stability, and hence affect the response to local dynamical

forcing. This mechanism implies a clear active role for ice precipitation in the mesoscale dynamics of weather systems which must be appreciated to develop our quantitative understanding beyond the limitations of current conceptual models.

In Section 2 we briefly review the sublimation process and the key results of the earlier works of CF and Harris (1977) in non-technical terms, with emphasis on the relevant time and depth scales.
Section **3** provides an overview of the development of the system observed in IOP 16 and its essential dynamics. In
Section **4** we show the mesoscale symptoms of sublimation in analyses of dropsonde observations, while Section 5 presents the results of the model simulations. In Section 6 we propose a hypothesis extending our results to the effects of sublimation to frontal waves more generally. In Section 7 we summarise our results and discuss their implications both for NWP and our understanding of weather system structure.

Section 2

Sublimation effects in weather systems

a) Process rates

The microscale physics of sublimation is simple and well established. However its operation in the atmosphere is dynamically interactive, quite complex and very little documented. A number of key features can be deduced from thermodynamic and kinetic principles. In this section we discuss these

principles to give some appreciation of the time and depth scales of sublimation without recourse to detailed calculation. This will prove a necessary background to our later observational discussion.

Microscopically, sublimation is the transfer of molecules from the ice crystal lattice to the gas phase, the reverse of the condensation process by which crystals grow directly from the gas phase. Both processes are given by the following equation for the rate of change of mass of an ice crystal with time:

$$\frac{dM}{dt} = C \times F \times \frac{S}{(L/KT)(L/RT - 1) + RT/eD}$$

The rate equation is represented as a product of three terms; the capacitance, the ventilation factor, and the environmental factor. The capacitance, C, is solely a function of ice crystal geometry. The ventilation factor, F, represents the enhancement of the diffusion mass growth rate when ice crystals are falling in the atmosphere and depends on crystal geometry, fall velocity and the ambient air density. The third term represents the effect of the environment on the growth rate and is independent of crystal geometry. The diffusion of water vapour towards the ice crystal and the thermal conduction of latent heat of sublimation away from the crystal are both represented in this term, where S is the supersaturation of water vapour in the environmental air with respect to ice, L is the latent heat of condensation or sublimation, T is the temperature of the environmental air, e is the saturation vapour pressure with respect to ice, D is the diffusivity of water vapour in air, K is the thermal conductivity of air, and R is the universal gas constant.

While temperature and pressure are important factors in determining the ice crystal growth rate, atmospheric variations tend to be dominated by the supersaturation with respect to ice, S.

Despite the low temperatures diffusion is rapid because it involves molecular transfer over microscopic distances with only a minor energy barrier due to intermolecular forces. Thus sub-zero precipitation in frontal weather systems is normally crystalline, with a variable degree of riming because the rate of condensation growth of ice is roughly sufficient to balance the provision of supersaturation by mesoscale ascent, which is typically of order 20-30 cms^{-1} or less (Rutledge and Hobbs, 1983).

The sublimation of snow can potentially proceed more rapidly than its growth by diffusion. This can be seen by considering the limitations imposed by humidity. The upper limit on the subsaturation is 100%, whereas the supersaturation with respect to ice in the atmosphere is limited by water saturation, a smaller amount varying between 0% at 0°C and 47% at -40°C, as shown in Figure 1.

Further, as CF remark, since the saturation vapour pressure increases with temperature the potential cooling due to sublimation must also maximise near 0°C. For modelling this has the significant implication that representation of the correct phase of cloud and precipitation in the range 0 to -10°C is thus important for accurate calculation of the effects of sublimation in the atmosphere.

The above arguments indicate the rapidity of sublimation. Precise particle calculations indicate that the 1/e-folding time for typical ice crystals is of order minutes at 60% saturation (CF). It is shorter than the time scale for evaporation of droplets because of the increased surface area of ice particles of the same mass. The sublimation depth scale is also shallow, frequently much less than 1 km, because of the low terminal velocity of ice crystals compared to raindrops or graupel. The density and terminal velocity effects thus combine to render sublimation generally more important than rain or hail evaporation in frontal wave dynamics.

Two further microphysical properties are important. Firstly, the different particle characteristics of snow and rain lead to very different atmospheric behaviour (CF). The evaporation of rain at modest rainfall rates is inhibited by the loss of the small drops which contribute most to the mass loss. This does not occur for snow. The bulk density of snow is approximately proportional to 1/D for particles of diameter D (Locatelli and Hobbs, 1974), so that the mass loss is uniformly distributed across the spectrum (CF), rather than being greatest for small particles as in the case of rain. This behaviour is probably an important factor in the formation of multiple layers of cloud and associated temperature and moisture fluctuations frequently observed in frontal systems (GEWEX, 1996)

b) Thermodynamic and Dynamical effects

When saturated air parcels rise, latent heat of condensation is released immediately into the air in moist adiabatic ascent. If an air parcel laden with

precipitation were to descend then that process would also be moist adiabatic if the descent rate were small enough for evaporation or sublimation to keep pace. The process would occur spontaneously, being thermodynamically reversible. The critical question then is one of kinetics: how rapidly in practice can an air parcel descend while remaining essentially saturated?

As noted in the introduction, CF indicated that for sublimation this descent rate is potentially 20-30 cms^{-1}, enough to support typical mesoscale circulations. The critical point to note, however, is that since the process is spontaneous it corresponds to an atmospheric instability, since an infinitesimal downward perturbation of such an airmass will induce a subsaturation, hence cooling and further descent until all precipitation has fallen through or evaporated. Thus the instability has finite amplitude determined primarily by the microphysical characteristics.

The process of sublimation then reflects a tendency to maintain saturation with respect to ice despite the drying influence of descent in stable environments; in neutral to unstable conditions mixing and overall drying in terms of relative humidity results. Also, the Bergeron process presents a tendency of the atmosphere to attain ice saturation rather than water saturation in ascent above the melting layer in weather systems. Figure 1 shows the distribution of relative humidity with respect to ice *vs* temperature for all of the Vaisala GPS dropsondes used by the Meteorological Office's C-130 aircraft in FASTEX. The concentration of observations near 100% clearly indicates the powerful influence of the ice deposition/sublimation mechanism.

The next issue to consider is the environmental constraints operating on a sublimation-cooled, therefore denser, air parcel. Clearly the static stability is likely to be an inhibiting factor in general. Harris (1977) considered the local situation of ice streams evaporating into a near-neutral environment. Without dynamical feedback the cooling is clearly greatest immediately beneath the cloud and so a stable layer results above a layer with weak stability. As precipitation continues the lower layer is progressively destabilised until it becomes super-adiabatic and cooling-driven convection breaks out. Harris demonstrated that this could occur through a 400 m layer within 1 hour with typical precipitation rates of the order of $0.1 mmh^{-1}$. Downdraughts of several ms^{-1} were predicted by a 1-dimensional dynamical model, which showed significant dependence upon the assumed particle characteristics.

In these neutral-unstable conditions air parcels paradoxically are dried by the sublimation in the sense that their relative humidity is reduced by the ensuing descent. For such air parcels within frontal environments this process might progressively produce deep layers of near-neutral air. The determining factor is the time spent by such parcels in regions of substantial ice precipitation rates.

In stable frontal environments descent can most readily occur in slantwise trajectories, in frontal zones where latent heat release has reduced the moist potential vorticity and hence absolute momentum and θ_w surfaces are near parallel (Bennetts and Hoskins, 1979). The most evident observational features characterising this behaviour are strong localised forward cross-frontal circulations beneath frontal cloud in a sense corresponding to direct cooling (CF; Thorpe and Clough, 1991). The slantwise descent mechanism envisaged

by CF is schematised in Figure 2. From this schematisation it is evident that the relative humidity with respect to ice is a key indicator, since it must be slightly sub-saturated in order to cool and produce descent. (Note, also that the relative humidity is thus seen to be a consequence of the descent and ambient precipitation rate, rather than itself a determining quantity.) Unfortunately the limited accuracy of humidity measurements means that they do not provide a very strong test of the mechanism. A better check is provided by gradients of radar reflectivity indicating the depletion of precipitation, since they must occur through the same zone as the forward descent.

The role of terminal velocity is vital in determining the depth scale and intensity of sublimation effects. By imposing a layer of cooling beneath the layer warmed by latent heating the effect of sublimation is to undo part of the latent heat-driven dynamics in a pattern which may be expected to resemble a vertically oriented dipolar distribution of heating. Interestingly, such a distribution of potential vorticity from attribution principles may be expected to have rather localised response, primarily in static stability rather than vorticity (Hoskins et al, 1985), and so little direct effect might be expected in the surface pressure pattern.

Clearly the above precipitation effects are complex and involve substantial dynamical-thermodynamic interaction at the mesoscale. In view of this complexity there is a clear deficiency in the modelling literature in this area, which may well be needed to adequately parametrize the range of interactions and possible scenarios.

Section 3

The Event

The frontal wave studied in IOP 16 formed from a weak trough on the main baroclinic zone in the western Atlantic. The rearmost of two troughs, it passed Newfoundland around 06-12UTC on 16th February 1997 and travelled rapidly (30-40 ms^{-1}) across the Atlantic, deepening to form a low pressure centre in the first half of 17th February.

Figure 3 shows the development characterised in 3-hourly Meteosat infrared geostationary satellite images for the observation period overlaid with contours from the Meteorological Office's operational Limited Area Model (LAM) analyses. The Meteorological Office's operational LAM forecast beginning at 18UTC on 16th was used for flight planning the aircraft-based observations. This forecast was consistent with its predecessors and proved accurate, more so than the following 00UTC 17th forecast.

The trough deepens from 03UTC to form an emerging cloud head, which is clearly distinct from the upper cloud shield by 06UTC as shown in Figure 3b. Also in the interval the uniform rear part of the cloud shield thins in places to result in a pronounced set of bands, some of them parallel to the rear edge by 06UTC, clearly evident in Figure 4. From this stage the wave develops rapidly, forming a secondary cloud head between 10UTC and 11UTC (Figure 3d). The LAM indicates the formation of a closed low centre near 12UTC, though the sounding observations suggest that it probably occurred around 9-10UTC in the atmosphere.

The C-130 and P3 aircraft worked essentially to their pre-flight plan to map out 6 runs perpendicular to the wave's path and separated by about 100 km along the wave assuming a system speed of 27.6 ms^{-1} from 240º. These are indicated in Figure 3c, when displaced according to the system velocity. 62 dropsondes were deployed, of which 45 gave usable data. Important features from the first run are discussed here; sonde locations are shown on the 06UTC satellite image in Figure 4.

Section 4

Observed characteristics

a) Data

The sounding observations were made with 45 RD82 GPS dropsondes developed by Vaisala and flight-tested by the Meteorological Office. The temperature and humidity elements were capacitative sensors as in the standard RS80 radiosonde, while the pressure sensor was the recently developed Barocap silicon pressure transducer as in the new RS90 radiosonde. Winds were provided by the Vaisala GPS111 receiver module on board the sondes with Vaisala NWG201 processor cards on board the C-130.

The humidity observations appear much more consistent than those from earlier dropsonde observations. This judgement is based upon the increased density of relative humidity observations near the ice saturation curve shown in

Figure 1, which is qualitatively a reasonable property to expect for such environments where the Bergeron-Findeisen process is operating. Despite the improved consistency, however, a high frequency of values at water saturation or higher suggests that the observations may be 5-10% too high at the moist part of the range. Trials are ongoing to test the calibration of sensors of the same design.

The basic parameters from the dropsonde data (temperature, scalar wind components and humidity) were objectively analysed as 2-dimensional vertical cross-sections for each of the runs indicated in Figure 3c. The objective analysis uses a successive correction algorithm (Pedder 1993) with isentropic vs horizontal distance coordinates. Data is extracted on isentropic levels every 0.5 degC from each sounding for input to the objective analysis. The isentropic filtering scale used in the analysis is 1.5 degC, corresponding on average to a vertical scale of around 30hPa. The horizontal filtering scale is approximately twice the mean sounding separation (about 60km). Horizontal distances are shown as the projected distance onto the plane chosen to resolve vector quantities.

b) Run 1

The authors' attention was originally drawn to the characteristics of this run by the fact that the main observed frontal features discussed below were totally absent from the operational 19-level LAM forecast, despite the fact that the

model correctly forecast the overall development and pressure deepening. Since a good forecast is available the case is potentially most valuable to investigate the sensitivity to detailed processes.

Harris's (1977) study centred on the formation of a cooled layer at the base of an upper level cloud. A frontal surface is of course a typical location of such a feature, and a well-defined example occurs in run 1, though the cooling is not sufficient that convection is evident. This is illustrated in Figure 5, which shows cross-sections of key thermodynamic and kinematic quantities.

The cross-section of θ_w (Figure 5a) shows a modest low level gradient, but a particularly strong and coherent gradient is evident between 450 hPa and 550 hPa, corresponding to a frontal surface across several soundings. This may be more fully seen in the dry static stability, as seen in the Brunt-Vaisala frequency N^2, Figure 5b.

Beneath the stable frontal layer in Figure 5b is a substantial layer of reduced stability, becoming moist unstable beneath sondes 6 and 7. At full data resolution soundings 8, 9 and 11 possess shallow dry adiabatic layers immediately beneath the inversion, a typical symptom of sublimation cooling. The extent of the upper stability transition is striking, crossing the whole 440 km section and θ_w values from 10 to 13°C, suggesting that it may be formed by a process operating over the system's extent. It is suggested that sublimation from the upper cloud shield makes an important contribution to the presence and amplitude of such a structure. We will return to this point in the model studies below.

The cross-frontal flow shows particularly interesting structure (Figure 5c). A shallow layer of strong forward flow coincides with much of the stable zone of the upper front. The pattern in mid-troposphere shows a pair of forward-rearward flow near 500 hPa and another weaker pair at 650-700 hPa, with maxima of relative humidity (Figure 5d) above the peak forward flows, a pattern which qualitatively matches that predicted by the Clough-Franks mechanism.

The overall forward flow in the warm sector aloft is associated with the anticyclonic flow into the ridge strengthening downstream of the main latent heating zone. This probably corresponds to the reduction of potential vorticity above and downstream of the level of maximum latent heating, which is also consistent with model diagnostics to be shown later. The local maximum in the frontal surface corresponds to a direct circulation driven by local sublimation cooling, and the fact that the maximum coincides with the lower part of the saturated region is consistent with CF's proposal of moist adiabatic descent occurring where precipitation is sufficient to support it. The layer is shallow because the available precipitation sublimes efficiently but is insufficient to support a deep layer of descent, hence the structure degenerates into finer scales because of the moisture distribution.

Figure 5e shows the along front flow and Figure 5f the associated momentum, v + fx. From theory the large tilt of the momentum surfaces through the upper front is normally associated with a low potential vorticity (or moist potential vorticity) value where momentum and θ or θ_w surfaces tend to become parallel. The 2-dimensional estimate of potential vorticity is not sufficiently reliable in the

curved flow to confirm this, but we note that the main region of large tilt coincides with the frontal region of both high and low static stability, while a similar but weaker secondary structure is evident at 650-700 hPa. The tilt is consistent with the occurrence of a strong cross-frontal circulation, if interpreted in a simple 2-dimensional sense. We shall return to this in considering the model results where full 3-dimensional diagnosis is possible.

The deepest area of weak stability around sondes 6 and 7 corresponds to a gap between cloud bands in Figure 4, which is also evident as an absence of ice particles in the aircraft data, with concentration maxima on either side. It seems likely that this gap is a consequence of sublimation-induced cooling occurring from the cloud shield over a long period, leaving a dissipating upper cloud band towards the cold side of sonde 7. The potential for sublimation clearly increases with the depth of the ice cloud layer which increases towards the warm air. Sonde 6 then effectively corresponds to the rear edge of the main cloud mass. It is interesting to note the distinct vertically aligned transition in the cross-front flow (Figure 5c). The velocity pattern, though only based on 2-dimensional information, suggests that a band of divergence is associated with this edge, a symptom also highlighted by CF in Fronts 87 observations as implying descent within the rear cloud edge. The parallel Doppler radar observations when available should be able to verify this interpretation in 3 dimensions.

It is helpful to consider how the gap between the cloud bands might form. Assume that the primary driving of such structure is latent heating and hence

ascent, which will be slantwise in the presence of thermal wind shear. This will form ice precipitation, which may then fall into regions which are not forced to ascend. By the mechanism discussed in Section 2 this will cause sublimation, cooling and hence descent which, in statically stable conditions must also be slantwise. Since, as we noted in Section 2, air at higher temperatures can take up more vapour, and hence cooling, we anticipate that the effect will be driven most strongly from the upper part of the melting layer and the region above it. This mechanism is thus essentially pulling the circulation from below, and the result is to evacuate a region where the descent is such that hydrostatically the source of the upper cloud is cut off and so a clear band is produced.

The mechanism we have just described seems to be unavoidably an evolutionary and dissipative one in realistic systems. A steady state might be envisaged in the form of a mode progressing towards warm air in which air ascends at the leading edge to drive the descending circulation towards its rear. Since, however, the precipitation falls downstream of the ascent in windshear, the descending part of the circulation does not precisely underlie the ascending and so a mesoscale break-up in structure is to be expected. The representation of such a coherent mesoscale internal structure appears to represent a significant problem to numerical forecasting because its scales are close to typical mesoscale grid meshes both horizontally and vertically, but below those of coarser models.

Section 5

Model studies

a) Model experiments

Model experiments were carried out with the original LAM version of the Unified Model (Cullen, 1993) and high resolution mesoscale versions initialised from the LAM at 21UTC on 16th February 1997. The model details are set out in Table 1.

Run:	Gridlength km	Number of levels	Precipitation scheme	Special features
A	50	19	Single phase	
B	11	45	Mixed phase	
C	11	45	Mixed phase	Sublimation cooling off

The model experiments were carried out as follows:

The LAM integration A was equivalent to the 18Z 16th Feb operational LAM forecast run and carried out using the same model configuration though updated physics routines. The grid length was approx 50km and there were 19 vertical levels. It was carried out using the original operational data (ie. a start dump from the previous LAM integration, boundary conditions from the global

model and observations files) and run out to 15Z on the 17th. This integration used the cloud scheme then in use in the model, which treated water as vapour or liquid prognostically and diagnosed ice. Experiments with the LAM using the new mixed phase cloud and precipitation scheme produced very similar results in regard to the features of interest here.

The Mesoscale integrations B and C were carried out on a 229 x 158 point 11 km grid, corresponding to that currently operational in the Meteorological Office, though vertical level. The horizontal domain was determined by the need to keep the fast moving system within the domain for the times of interest. 45 vertical levels were used, most of which were the same as are used in the current operational 38 level mesoscale model but with extra levels in mid-troposphere (the region of interest in this study) to bring the maximum spacing down to about 30mb at 700mb. The integrations were initialised from the LAM experiment A. Fields at 21Z and the boundary conditions were also obtained from this integration. The experiment was run as far as 12Z, the times being chosen so that the surface feature rapidly develops from a trough to a closed low within the integration period. The two mesoscale integrations used a mixed phase cloud scheme (Wilson and Ballard, 1998) which treats liquid and ice water as prognostic variables and attempts to explicitly model the various phase transitions and interactions, including sublimation. For all three integrations a number of key dynamical variables were output on model levels and then processed with a diagnostic package to interpolate onto 25 hPa pressure levels and generate derived quantities.

It should be noted that the precipitation scheme only carries one ice phase variable, which is given a mean terminal velocity so no suspended ice cloud is represented.

b) Results

Figure 6 illustrates overall performance of the three model integrations. Figures 6a, b and c show the simulated temperature of the model ice cloud top at 12UTC on 17th February 1997 with mean sea level pressure superimposed. Figure 6d shows a Meteosat infrared image for the same time and marks the pressure centre deduced from measurements made by the NOAA P3. The model integrations all agree in the trajectory of the low pressure centre up to 12Z, though satellite imagery suggests that the model system may be around 150 km ahead of the observed system. It is evident also that all models, including the LAM, (Figure 6b) have captured the overall depth of the system. The low simulated cloud tops south of the low centre suggest that the model has excessive descent tending to form too strong a dry intrusion, a view which is confirmed by the humidity pattern in dropsonde cross-sections for the middle runs (not illustrated).

The two mesoscale simulations are characterised by sharper pressure gradients than the LAM, and they differ in the structure of the cloud head and the associated surface pressure pattern. The full simulation (Figure 6b) shows rather more structure, including the differentiation of two cloud heads and a tighter frontal trough closely followed by pronounced ridging, indicating that

sublimation cooling plays an important role in determining mesoscale structure. The similarity of forecast central pressures seems to follow essentially the insensitive behaviour we predicted in Section 2 on the basis of latent heat exchanges due to condensation and sublimation.

The difference between the mesoscale integrations is brought out more fully in Figure 7, which shows the 950 hPa vorticity. Vectors of the difference in winds between integrations B and Care overplotted, and these display differences up to 15ms^{-1} associated particularly with the differences in cold and warm front locations and strength. The vorticity values in the two integrations show a corresponding difference; in the presence of the sublimation stronger and more distinct bands of positive and especially negative values are evident (not illustrated). Clearly then the main effect of sublimation in the model is not simply a thermodynamic one but because of the internal adjustment to thermal wind balance a difference in the circulation transpires and a significant change in the frontogenesis.

We next consider the structure of simulated cross-sections compared to the observations discussed in Section 3. Because the model integrations do not exactly reproduce the observed system the comparison between values simulated at the exact time and location may not be appropriate. Since the features discussed earlier only occur in run 1 in a region of the system which shows distinct along front structure this point is significant. In fact the mesoscale experiments both show a frontal surface which extends for a substantial distance along the system. The model cross-sections are taken along the line AB marked in Figure 11, which is perhaps 150 km ahead of the

observed system to match the estimated displacement of the simulated system. The differences between model integrations are somewhat greater at this location than at the exactly collocated position, but the modelled structures are qualitatively similar at both positions.

i) LAM experiment A

Figure 8 shows a set of cross-sections from the LAM experiment in a comparable system location to the observations shown in Figure 5. There are increased gradients in θ_w, momentum and other quantities in the vicinity of the front, but the humidity structure (Figure 8d) is bland, and the overall gradients do not increase dramatically. These features are most probably limited by the model's low vertical resolution and incapacity to represent the fine vertical scales of frontogenesis or sublimation in mid-troposphere. There is formation of layers with fairly strong and weak static stability in Figure 8b, but they differ substantially from those observed. The gradients tilt in an opposite sense to that observed, and the depths through which the layers extend are much greater than those in the atmosphere. They thus correspond to regions of instability distorted and vertically displaced probably because of the model's inability to resolve sublimation adequately. The moist static stability from Figure 8a shows no convective instability other than immediately above the sea surface whereas the observations show two distinct localised zones of mid-level convective instability around 600 hPa and 700 hPa.

The cross-frontal flow in Figure 8c lacks the strong gradients evident in the atmosphere, particularly in mid-troposphere, and has no feature comparable to the shallow forward flow above the front. Comparing the momentum cross-sections in Figure 8f, the contrast between resolvable strong and weak gradients marking zones of modest and low symmetric stability is suggested but not well captured.

ii) Mesoscale model experiment B

The results of experiment B are illustrated in Figure 9. These cross-sections bear a clear structural similarity to those shown in Figure 5, and have well defined mesoscale humidity variations and internal structure. Sloping layers of high and low static stability are now present (Figure 9b), though they occur at a level almost 100 hPa below those observed. The level and depth of the regions of high and low static stability relative to the upper front agree with the observations much better than experiment A.

Collocated with the sloping layer of strong static stability, though more extensive, is a shallow layer of increased forward descending flow (Figure 9c) in the upper front. It is weaker than observed, but qualitatively similar and in a similar location relative to the thermal gradient. The humidity pattern shows some qualitative similarity to the observed humidity variations, and the region of the strong forward flow possesses a gradient with values decreasing from 100% to around 98% saturated with respect to ice, very much in line with the predictions of CF. However, the model variations are rather smaller in

amplitude than the observed humidity fluctuations and also show much smaller supersaturation with respect to ice, a feature also shared by the other runs. This suggests that the model moisture scheme may have a significant deficiency on NWP time scales; with limited potential instability much of the moisture transport at this resolution would be expected to occur on or near to resolved scales. If it indeed represents a systematic bias it implies rather different mesoscale precipitation intensity and moisture-driven transfers in mid-troposphere. Note that surface precipitation may not be dramatically affected by such an error since most of the water content in the column occurs near the surface; nonetheless the dynamical effects highlighted by this work would be inadequately represented if the observed supersaturation and precipitation rates aloft are not achieved.

Figures 9e and 9f show the along-front velocity and momentum, the latter of which shows strong tilt through the upper front much like that observed qualitatively, though the level of strong windshear also is too low. Since momentum is conserved in two dimensional flow the strong tilt would be associated with a direct cross-frontal circulation, which is the case here. Thus if our dynamical coupling interpretation holds it quite seems possible that the deficiency in the height of the thermodynamic structure could feed into the jet and momentum structure through the cross-frontal flow.

The difference in the level of occurrence of the front is difficult to account for in detail, as fronts are a complex dynamical phenomenon. Although the frontal surface slopes, it does not rise anywhere to the height of the observed surface.

However, the model system has only evolved with high vertical resolution for 9 hours, whereas the previous history of the system has been subject to the effects of the limited LAM resolution. Since the frontal symptoms and circulations shown in the cross-sections are clearly highly coupled it seems likely that the errors in representing the cloud and dynamical processes are already incorrect in the model field at the initial time, given that the trough system itself has a lifetime of a day or two before the deepening stage.

iii) Mesoscale model experiment C

Figure 10 presents the cross-sectional structure of this model simulation, in which the thermodynamic effect, ie. cooling due to sublimation has been omitted.

It is evident in both Figures 10a and 10b that the strong contrast between weakly and strongly stable zones in experiment B is reduced. Also the shallow forward descending flow is much weaker in Figure 10c, and the amplitude of the humidity variations is reduced. Thus the stability and circulation symptoms that we have associated diagnostically with the sublimation are indeed both associated with sublimation in the model, and a pronounced sensitivity of the flow results.

Figure 10f, however, shows that the structure of momentum surfaces is much more like that of experiment B than that of experiment A. Theoretically, the momentum surfaces are most directly associated with the potential vorticity, or moist potential vorticity, which determines the Jacobian constraining their tilts

compared to the potential temperature distribution in two dimensions (Bennetts and Hoskins, 1979). Figures 11 and 12 illustrate the potential vorticity structure. Figure 11 shows a plan view of potential vorticity at 525 hPa with the location of vertical cross-sections marked. In Figure 11 it can be seen that substantial negative potential vorticity minima are quite close to the selected cross-sections, which are associated with the upper part of the main latent heating region. Figure 12 shows that the potential vorticity in the vicinity of the greatest tilts is negative in both experiments B and C. The low value presumably results as the upper part of the dipolar anomaly characteristically associated with latent heating. The value reached in experiment B is significantly smaller, about -2 PVU, though the patterns in runs B and C are qualitatively similar. The occurrence of a significant region of negative potential vorticity implies that symmetric instability is possible in this location. This may be problematic since the model's vertical resolution is less than that found necessary by Persson and Warner (1993) to properly resolve symmetrically unstable circulations. Higher resolution, however, is not practical at the present time.

The vertical velocity cross-sections from the model experiments B and C are shown in Figure 13. As expected from the horizontal flow both experiments possess shallow regions of descent coincident with the forward flow, and the descent in experiment B is greater by a factor around 2. Figure 14 shows the cross-section of moist static stability N_m^2 from experiment B. The effective static stability, N_m in this moist case, is smaller than the dry static stability which applies in experiment C (Figure 16b) in the forward flow by a factor of around 1.7. This behaviour also is consistent with moist adiabatic descent in

precipitation, noting that the forcing of descent has been increased slightly because of the lower negative potential vorticity values (ie. more anticyclonic flow) in run B. With this allowance our results confirm in all respects that CF's prediction of moist slantwise descent provides a consistent account of both the atmospheric and model results.

Section 6

A sublimation hypothesis for weather system structure

It is possible to generalise from the results above. Since ice precipitation is usually a concomitant of ascent in frontal waves, sublimation potentially provides a feedback by which any forcing of ascent potentially also forces descent, and this descent must occur on the mesoscale because of the short length and time scales of precipitation itself.

By this mechanism ice precipitation provides downward transfer of dynamical influence by its presence directly, and possibly hydrostatic adjustment to the cooling will imply some upward influence also. Since precipitation falls downstream it may be a means of transferring the effects of forcing through mesoscale distances downstream in a system, and also across stream if it operates in conjunction with slantwise ascent or descent.

The above processes thus provide a precisely defined means by which ascent and hence precipitation, while not necessarily mesoscale in origin, will have associated with it parasitic mesoscale substructure, as is commonly observed,

without the need to hypothesise the action of a mesoscale dynamical instability such as CSI. (There is also much evidence for the important role of melting in organising mesoscale structure of strongly precipitating frontal waves, as demonstrated by Stewart and co-workers (eg. Szeto and Stewart, 1997)).

We therefore make a sublimation hypothesis, that sublimation is normally associated with the formation of broad rainbands in middle latitude frontal systems. This process model has some features to commend it. In particular it is distinct from current conceptual models in being process-specific, conservative (in that it accounts for the coupled changes in all conserved variables including moisture) and indicating quite specifically the circumstances in which it will occur, the limits on its amplitude and the necessary observables for verification. These observables include the conventional dynamical variables and the distribution and properties of ice precipitation observable in aircraft or radar measurements.

Section 7

Conclusions

In this study we have provided clear observational and model evidence of the importance of sublimation in producing mesoscale dynamical structure, and to that extent it follows condensation in the hierarchy of dynamical processes of frontal waves. The structure coincides with that predicted by Clough and Franks (1991) from microphysical calculations and dynamical arguments, in

particular in confirming that sublimation can support moist adiabatic slantwise descent, thus providing an enabling machinery for the development of mesoscale precipitation bands. This hypothesis was confirmed by omitting sublimation cooling from the model, which led to a substantial weakening of the principal symptoms in static stability and circulation.

The close correlation between the observed and modelled cross-frontal circulation and the moisture distribution strongly suggests that microphysical characteristics provide a major factor in determining the mesoscale dynamical structure of frontal waves. Since current cloud/precipitation parametrisations have been little optimised with regard to microphysical characteristics and the ambient conditions they may thus prove to be a key element in improving NWP using high quality data such as those available from FASTEX.

Our results have several important implications for our understanding and forecasting of frontal waves.

- We remarked that the strong feedback between descent and sublimation cooling amounts to a kinetic instability of the system, since in the presence of ice precipitation any forcing for descent will be amplified up to a limit determined by the precipitation rate. We suggest that this be referred to as Sublimation Enhanced Descent (SED), noting that it is akin to instability but its behaviour is quite different physically and mathematically from the fluid dynamic instabilities normally encountered in meteorology. In view of the active coupling role of ice precipitation we also suggest that the precipitation should properly be viewed as a dynamical variable of the system to be measured where possible along with the other thermodynamic elements.

- The frontal circulation and static stability structure was found to be sensitive to sublimation, which thus provides important verifiable links between observed thermodynamic and dynamical structure and the fundamental microphysical processes and precipitation structure of the model. Since CF have shown that the dynamical effects of sublimation are limited by the concentration of precipitation a sensitivity to the whole vertical profile of precipitation and its terminal velocity is evident.

- Our results suggest that the system studied behaves approximately linearly in the imposed forcing, in that the vertical velocity increased by about a factor of two when effective static stability N decreased by 1.7, using the appropriate static stability for the conditions, which can be moist adiabatic while sublimation of snow is sufficient to support it.

- In our model simulations symmetric instability (SI) arose as a local outcome of diabatic processes, rather than itself driving the system's overall behaviour on a larger scale. This is encouraging from the point of view of understanding weather system development, since stable forcing/response systems are much more readily understood and quantitatively forecast than the growth of inherently unstable modes. Negative potential vorticity was found to be present without sublimation but was appreciably enhanced by the sublimation cooling because of the associated anticyclonic descending motion in the moist warm sector environment. The forecasting problem in this situation thus appears to be one of internal complexity and possibly model resolution rather than unpredictability in this regard. In the whole set

of aircraft runs it was evident, though not illustrated here, that the model underpredicted the observed tendency to forward descending motion in the south-western quadrant of the system. This may have been associated with deficiencies in modelling the microphysics, though further investigation is necessary to confirm this possibility.

- We contend then that the driving of mesoscale structuring of this system is best described by the formalism of forcing and response rather than of inherent mesoscale instability. While the criterion for mesoscale dynamical instability is locally fulfilled the instability hypothesis does not in this case determine the structure of the system. Instead the pattern is determined by the diabatic processes, which thus constitute a clearer driving mechanism. The distinction is clearly a very important one because it firmly places the proper accounting for such structures in terms of dynamical forcing, and response via the ice precipitation, both of which factors are in principle well understood.

- The model results suggest that the atmospheric structure in the region observed should be studied closely in the radar and aircraft observations in order to refine our understanding of the atmosphere's response to such forcing in conditions probably unstable to SI or CSI. It is interesting to note that SI, if it indeed occurred in the atmosphere, is in the warm sector in mid-troposphere in the anticyclonic outflow from the main latent heating region, a location not usually considered to be of dynamical importance. However, at this location interactions between cloud physics and system dynamics are likely to be particularly important because of the long periods during

which mid-level air parcels may be modified within the ice precipitation envelope.

- We have interpreted this situation in direct physical terms and shown that model results also could be interpreted within a quantitative process framework, in which precipitation and sublimation played an explicit role. We thus recommend this means of interpreting weather system structure and evolution more generally, and remark that our inferences refer to symptoms that can be observed in satellite infrared and other imagery, including banding and mid-level fragmentation of the cloud.

There are however some important issues that we have not addressed here, some of which are the subject of ongoing work.

Our integrations for practical reasons of domain size and resolution have covered only a 9-15 hour period. Attempts are being made to initialise from earlier times to assess whether a better simulation will result from better resolution of the sublimation, and the overall role of sublimation in determining localised frontal structure within the system.

The situation described by Harris has not as yet arisen in an important way in the present case. Shallow layers of static instability were evident in some high resolution sonde data for this and other cases, but the present model simulations do not approach static instability aloft. The possibility that sublimation of ice precipitation may induce layers of instability remains to be

investigated. Its occurrence and distribution will depend upon the presence of air parcels which persistently encounter precipitation by travelling close to the system's velocity, a situation which must occur most often in the warm sector and warm frontal region aloft. Both are regions where banded precipitation frequently occurs at the surface, though very few studies have been made of the associated mesoscale structure aloft.

In demonstrating that the feature studied is amplified by sublimation-enhanced feedback, we transfer attention to the forcing process. It is possible for example to envisage that the simplest baroclinic system, an Eady wave forced only by boundary temperature perturbations, may generate a wealth of

mesoscale internal structure in which sublimation has operated upon any forcing for descent to amplify it within the precipitating regions. As in our preceding discussion the size of these effects will clearly be proportional to the strength of the vertical motion but also their distribution will depend upon the time for which air parcels receive ice precipitation and the intensity of precipitation.

Thus we focus attention upon the kinematic properties of the system and encounter an interesting corollary. Bretherton (1966) highlighted the importance of critical layer instability in the theoretical analysis of baroclinic instability. It is evident from our approach that the simplest Eady wave initially without internal structure can develop mesoscale structure via precipitation and sublimation, and that structure will tend to form in the vicinity of the wave's critical surface in mid-troposphere where the vertical motion is greatest. The shape of the critical

surface is thus likely to play a central role in the resulting mesoscale structure, as has been found in studies of larger scale frontogenesis (Hoskins and West, 1979; Davies et al, 1991). This prediction and its implications will be the subject of future work.

ACKNOWLEDGEMENTS

We wish to thank our JCMM colleagues and all of our collaborators in the FASTEX experiment which led to such a successful mission. In particular we are grateful to Steve Devereau, Pete Healey, John Reid and Nick Jackson of the Meteorological Research Flight and Andrew Macallan of JCMM for great efforts made to ensure the success of dropsonde operations, and the remainder of the Flight and Eddy Carroll of the National Meteorological Centre for their assistance in carrying out the flight and subsequent processing. Also we thank Tim Hewson and Dave Jorgensen and the forecasting, planning and US aircraft teams for their key roles in coordinating operations. We are also grateful to Mark Dixon for assistance in the objective analysis and Peter Panagi for provision of diagnostic programs used in the studies.

REFERENCES

Bennetts, D. A. and Hoskins, B. J. 1979 Conditional symmetric instability - a possible explanation for frontal rainbands. *Q. J. R. Meteorol. Soc.*, **105,** 945-962

Bretherton, F. 1966 Critical layer instability in baroclinic flows. *Q. J. R. Meteorol. Soc.*, **92,** 325-334

Clough, S. A. and Franks, R. A. A. 1991 The evaporation of frontal and other stratiform precipitation. *Q. J. R. Meteorol. Soc.*, **117**, 1057-1080

Cullen, M. J. P. 1993 The unified forecast/climate model. Meteor. Mag., **122**, 81-94

Davies, H. C., Schär, C. and Wernli, H. 1991 The palette of fronts within a baroclinic wave development. *J. Atm. Sci.*, **48**, 1666-1689

GEWEX 1996 World Climate Research Programme, Global energy and Water Cycle Experiment, GEWEX Cloud System Study, Working Group 3, Report and Recommendations, NASA Goddard Institute for Space Studies, 1-3 November 1995, WCRP Informal Report No. 9, June 1996

Harris, I. 1977 The effects of evaporation at the base of ice precipitation layers: theory and radar observations. *J Atm. Sci.*, **34**, 651-672

Hoskins, B. J. and West, N. V. 1979 Baroclinic waves and frontogenesis. Part II: Uniform potential vorticity jet flows - cold and warm fronts. *J. Atm. Sci.*, **36**, 1663-1680

Hoskins, B. J., McIntyre, M. E. and Robertson, A. W. 1985 On the use and significance of potential vorticity maps. *Q. J. R. Meteorol. Soc.*, **111**, 877-946

Joly, A, Dave Jorgensen, Shapiro, M. A., Thorpe, A., Bessemoulin, P., Browning, K. A., Cammas, J.-P., Chalon, J.-P., Clough, S. A., Emanuel, K. A., Eymard, L., Gall, R.. Hildebrand, P. H., Langland, R. H., Lemaitre, Y., Lynch, P., Moore, J., Persson, P. O. G., Snyder, C., and Wakimoto., R. M. 1997 The Fronts and Atlantic Storm-Track Experiment (FASTEX): Scientific Objectives and Experimental Design. *Bull. Amer. Meteor. Soc.*, **78**, 1917-1940

Locatelli, J, D., and Hobbs, P. V.	1974	Fall speeds and masses of solid precipitation particles. *J. Atm. Sci.*, **79**, 2185-2197
Marecal, V., and Lemaitre, Y.	1995	Importance of microphysical processes in the dynamics of a CSI mesoscale frontal cloud band. *Q. J. R. Meteorol. Soc.*, **121**, 301-318
Pedder, M. A.	1993	Interpolation and filtering of spatial observations using successive correction and Gaussian filters. *Mon. Wea. Rev.*, **121**, 2889-2902
Persson, P. O. G., and Warner, T. T.	1991	Model generation of spurious gravity waves due to inconsistency of the vertical and horizontal resolution.
Persson, P. O. G., and Warner, T. T.	1993	Nonlinear hydrostatic conditional symmetric instability: implications for numerical weather prediction. *Mon. Wea. Rev.*, **121**, 1821-1833
Rutledge, S. A., and Hobbs, P. V.	1983	The mesoscale and microscale structure of clouds and precipitation in midlatitude cyclones. VIII: A model for the "seeder-feeder" process in warm-frontal rainbands. *J. Atm. Sci.*, **40**, 1930-1949
Szeto, K. K., and Stewart, R. E.	1997	Effects of melting on frontogenesis. *J. Atm. Sci.*, **54**, 689-702

Wexler, R., and Atlas, D. 1958 Moisture supply and growth of stratiform precipitation. *J. Meteor.*, **15**, 531-538

Wilson, D. R., and Ballard, S. P. 1998 A microphysical based precipitation scheme for the U. K. Meteorological Office Unified Model. Submitted to *Quart. J. Royal Meteorol. Soc*

FIGURES

Figure 1 Scatter plot of relative humidity with respect to ice against temperature (degrees C) from all FASTEX C-130 dropsoundings. Data points are plotted approximately every 1.5 seconds.

Figure 2 Schematic of the Clough-Franks mechanism

Figure 3 Sequence of 3-hourly Meteosat IR images for 03 UTC to 12 UTC on 17/02/97, FASTEX IOP 16. The black contours are surface pressure from a UKMO Limited Area Model forecast starting at 18 UTC on 16/02/97, with contours at intervals of 8hPa. Grey shades range from lightest < -54C to darkest > +18C in 6C intervals. The cloud head starts to emerge around 03 UTC. The dashed line on the 09 UTC image shows the flight track of the UK C-130 aircraft spaced out in a frame relative to the velocity of the moving low pressure system around 09 UTC.

Figure 4 Meteosat IR image for 06 UTC on 17/02/97, zoomed view otherwise as at Figure 3. The locations are indicated of dropsondes

Figure 5 Cross-sections of

a) Theta-w

b) N^2

c) System-relative across-front wind

d) Relative humidity with respect to ice

e) System-relative along-front wind

f) Momentum, v+fx

Figure 6 Simulated satellite image with PMSL superposed A B C obs.

Figure 7 950 hPa vorticity expt B with vector wind difference B-C

Figure 8 Vertical cross-sections from experiment A along the line AB shown in Figure 11, showing:

a) Theta-w

b) N^2

c) System-relative across-front wind

d) Relative humidity with respect to ice

e) System-relative along-front wind

f) Momentum, v+fx

Figure 9 Vertical cross-sections from experiment B along the line AB shown in Figure 11, showing:

a) Theta-w

b) N^2

c) System-relative across-front wind

d) Supersaturation relative humidity with respect to ice

e) System-relative along-front wind

f) Momentum, v+fx

Figure 10 Vertical cross-sections from experiment C along the line AB shown in Figure 11, showing:

a) Theta-w

b) N^2

c) System-relative across-front wind

d) Relative humidity with respect to ice

e) System-relative along-front wind

f) momentum, v+fx

Figure 11 Potential vorticity at 525 hPa from experiment B showing location of cross-sections AB and CD

Figure 12 Run 1 Potential vorticity from experiments (a) B and (b) C along line AB

Figure 13 Run 1 Vertical velocity from experiments (a) B and (b) C along line AB

Figure 14 Run 1 Moist static stability from experiment B along line AB

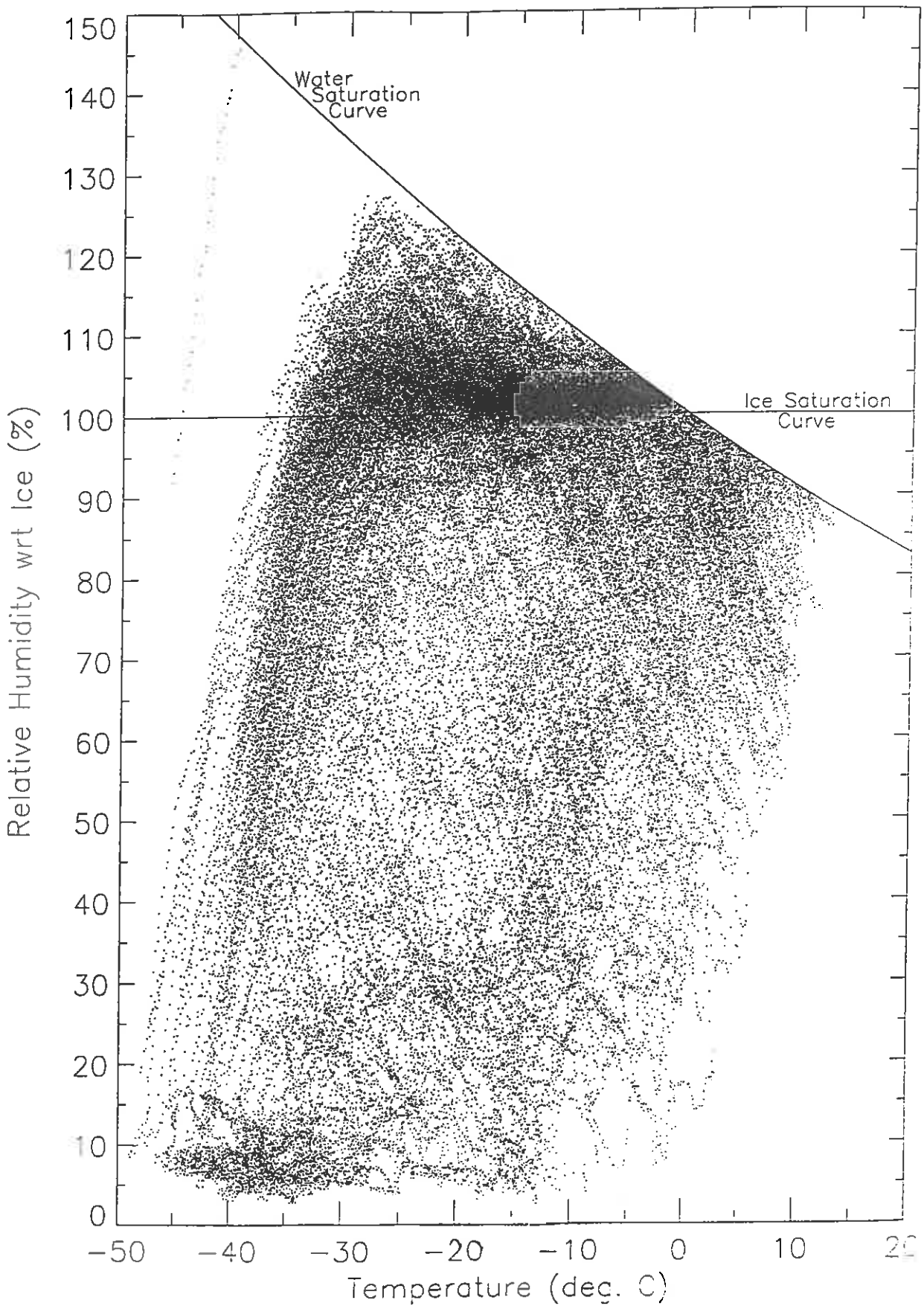
Water
Saturation
Curve
Ice Saturation
Curve
Relative Humidity wrt Ice (%)
Temperature (deg. C)
150
140
130
120
110
100
90
80
70
60
50
40
30
20
10
0
−50
−40
−30
−20
−10
0
10

Figure 1

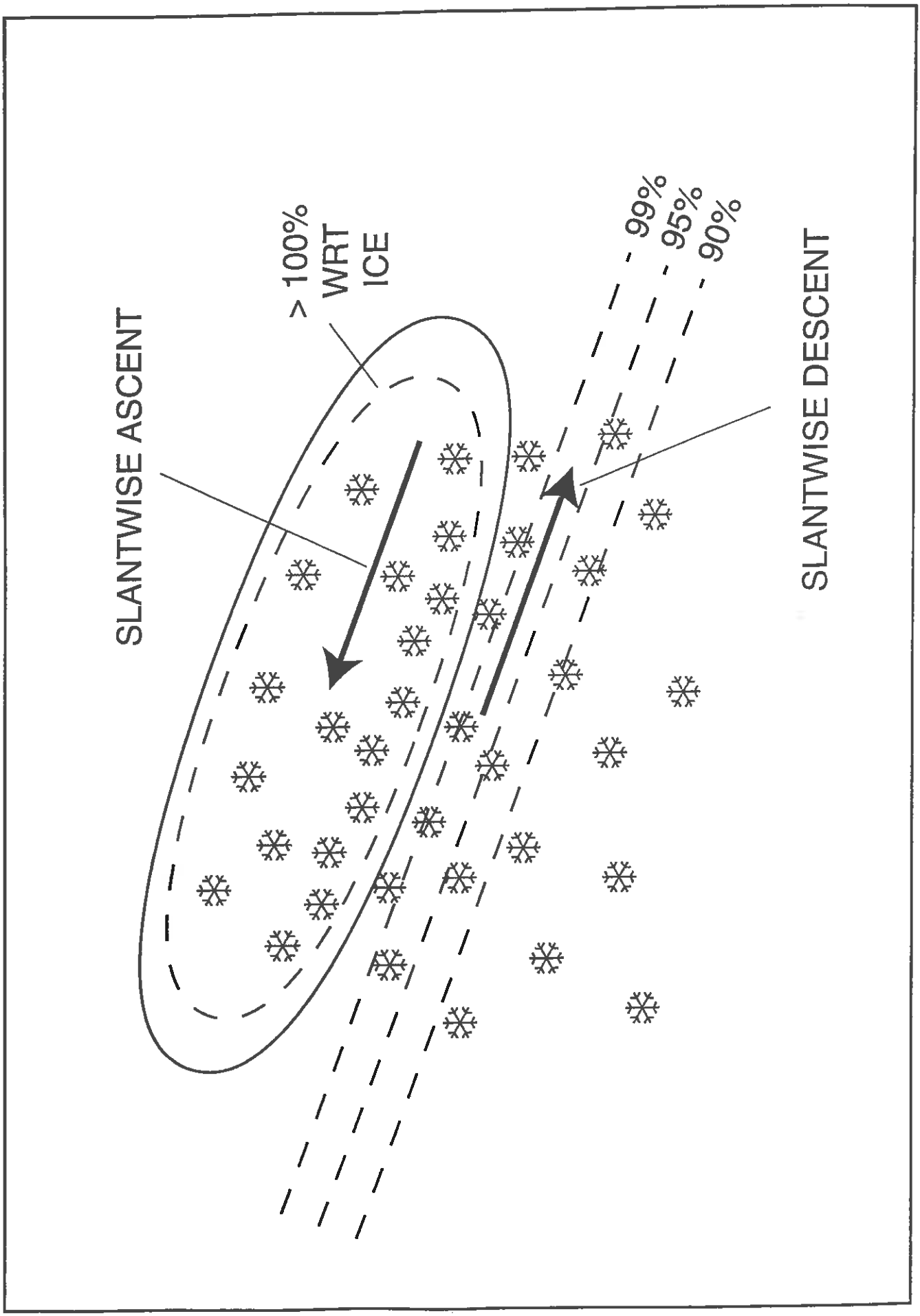

Figure 2

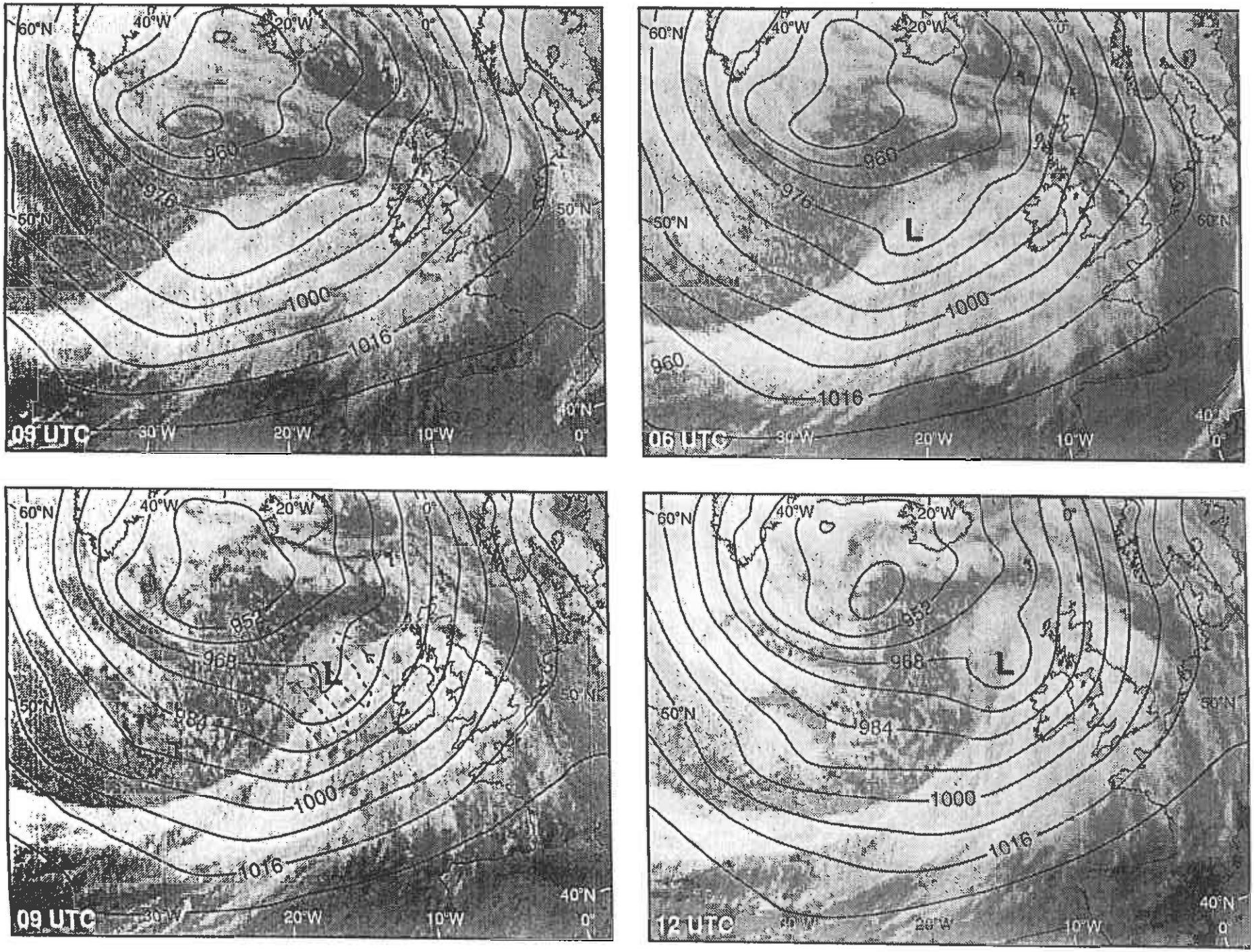
60°N
40°W
20°W
0°
960
976
50°N
1000
1016
40°N
09 UTC
30°W
20°W
10°W
0°
06 UTC
L
952
968
984
12 UTC

Figure 3

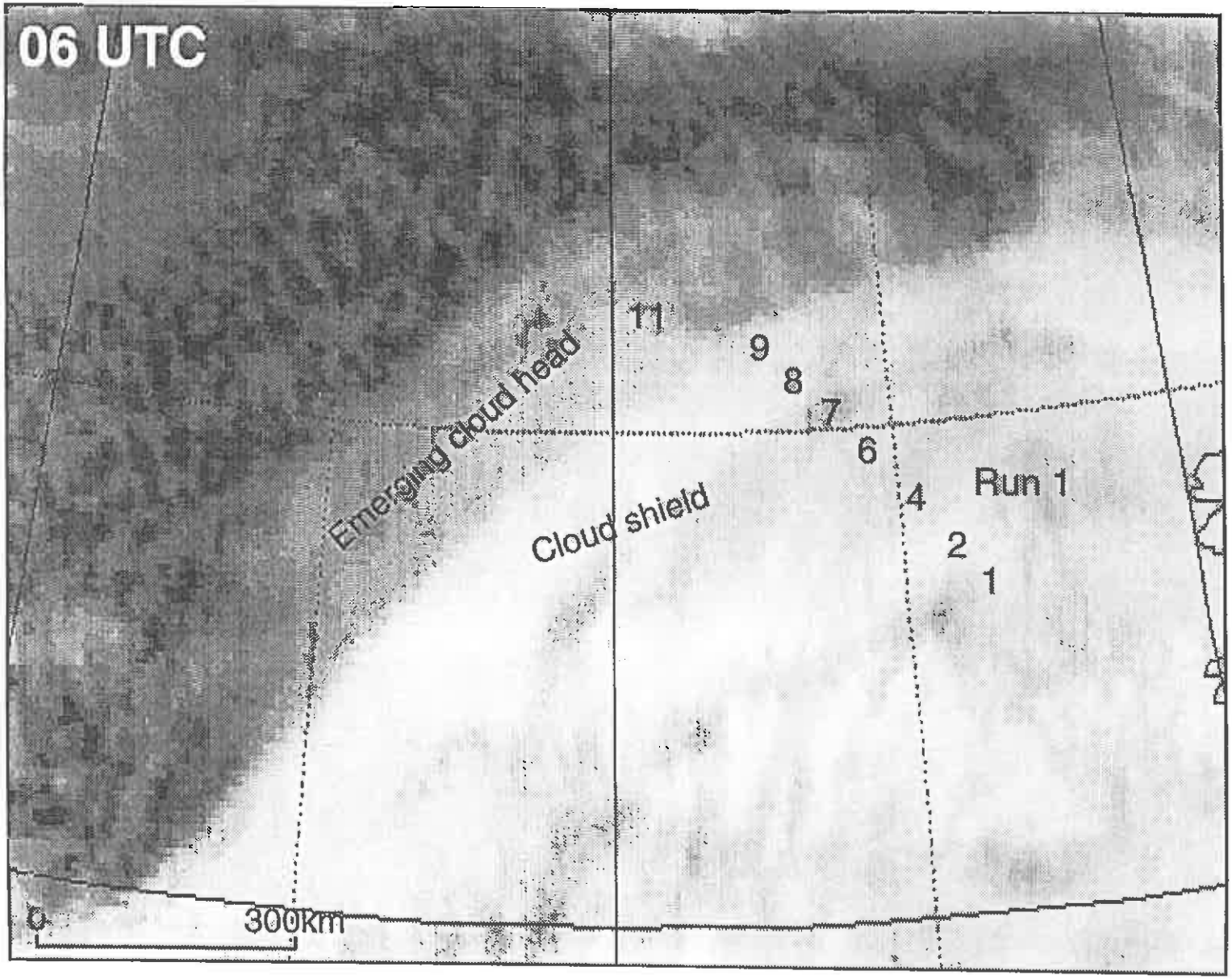
06 UTC
Emerging cloud head
Cloud shield
11
9
8
7
6
4
2
1
Run 1
0
300km

Figure 4

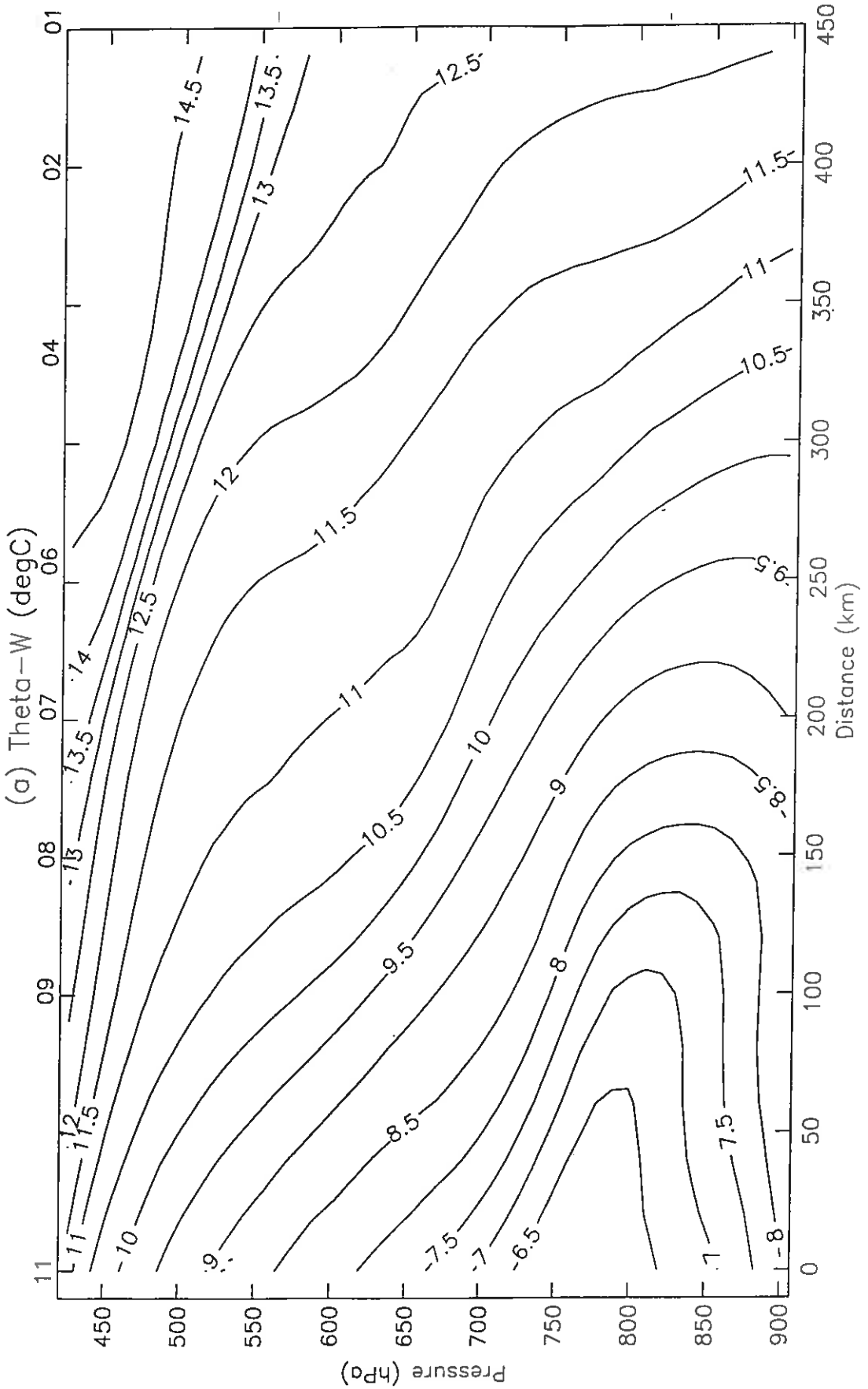
(a) Theta-W (degC)
Pressure (hPa)
Distance (km)
01
02
04
06
07
08
09
11
0
50
100
150
200
250
300
350
400
450
450
500
550
600
650
700
750
800
850
900
14.5
14
13.5
13
12.5
12
11.5
11
10.5
10
9.5
9
8.5
8
7.5
7
6.5

Figure 5a

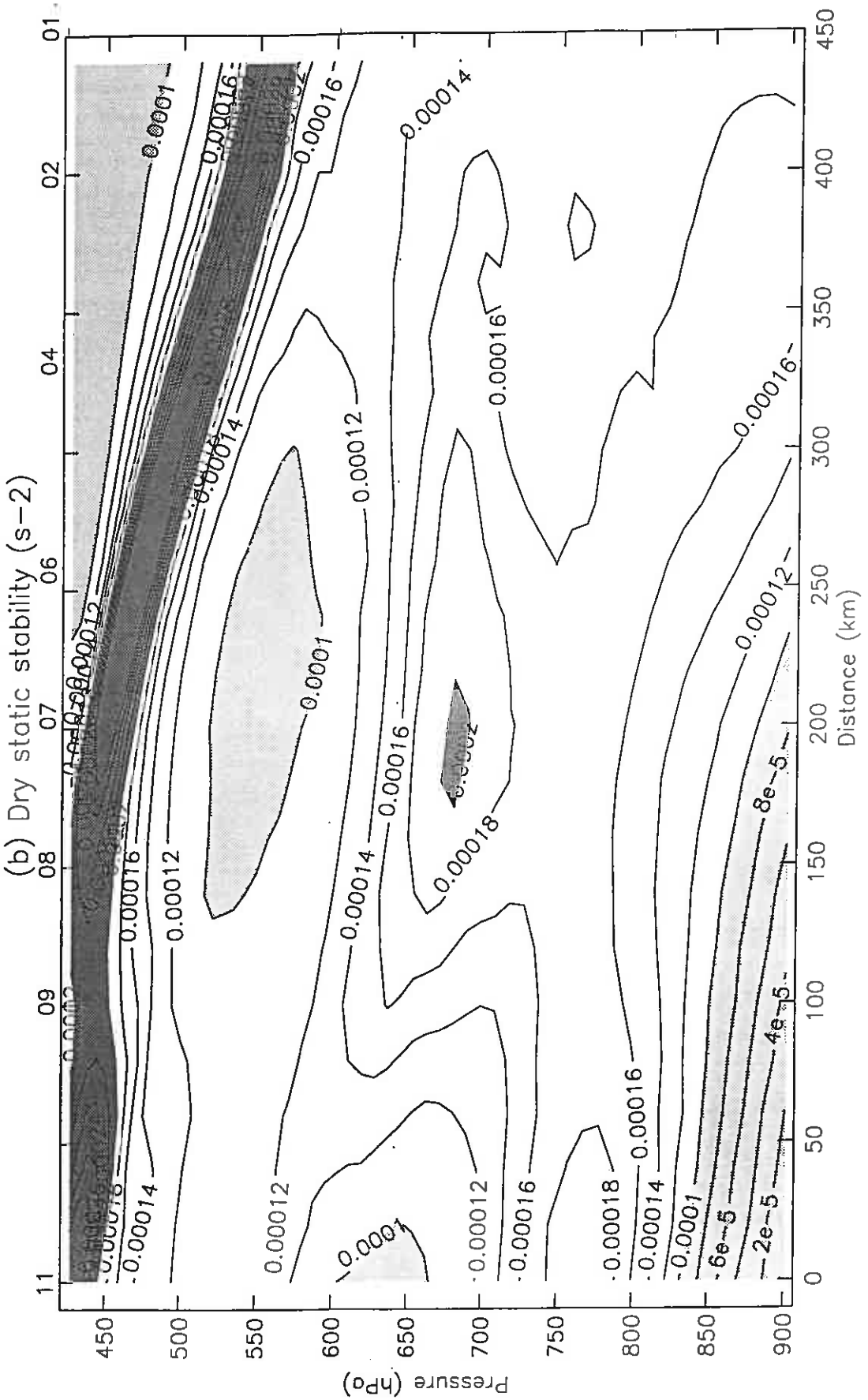
(b) Dry static stability (s−2)
Pressure (hPa)
Distance (km)
0.0001
0.00012
0.00014
0.00016
0.00018
8e−5
4e−5
2e−5
−6e−5
−0.0001
−0.00012
−0.00014
−0.00016
−0.00018

Figure 5b

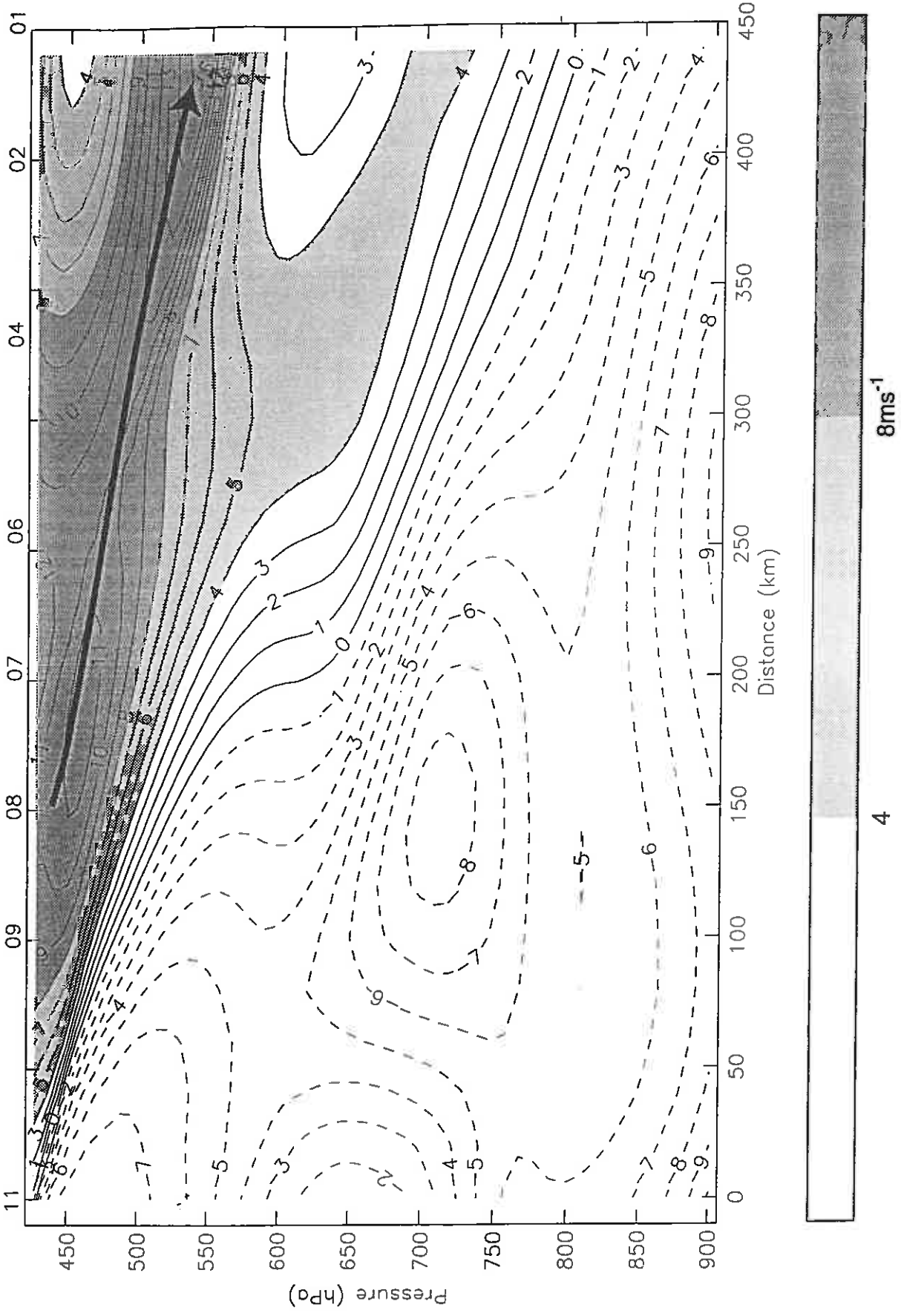

Figure 5c

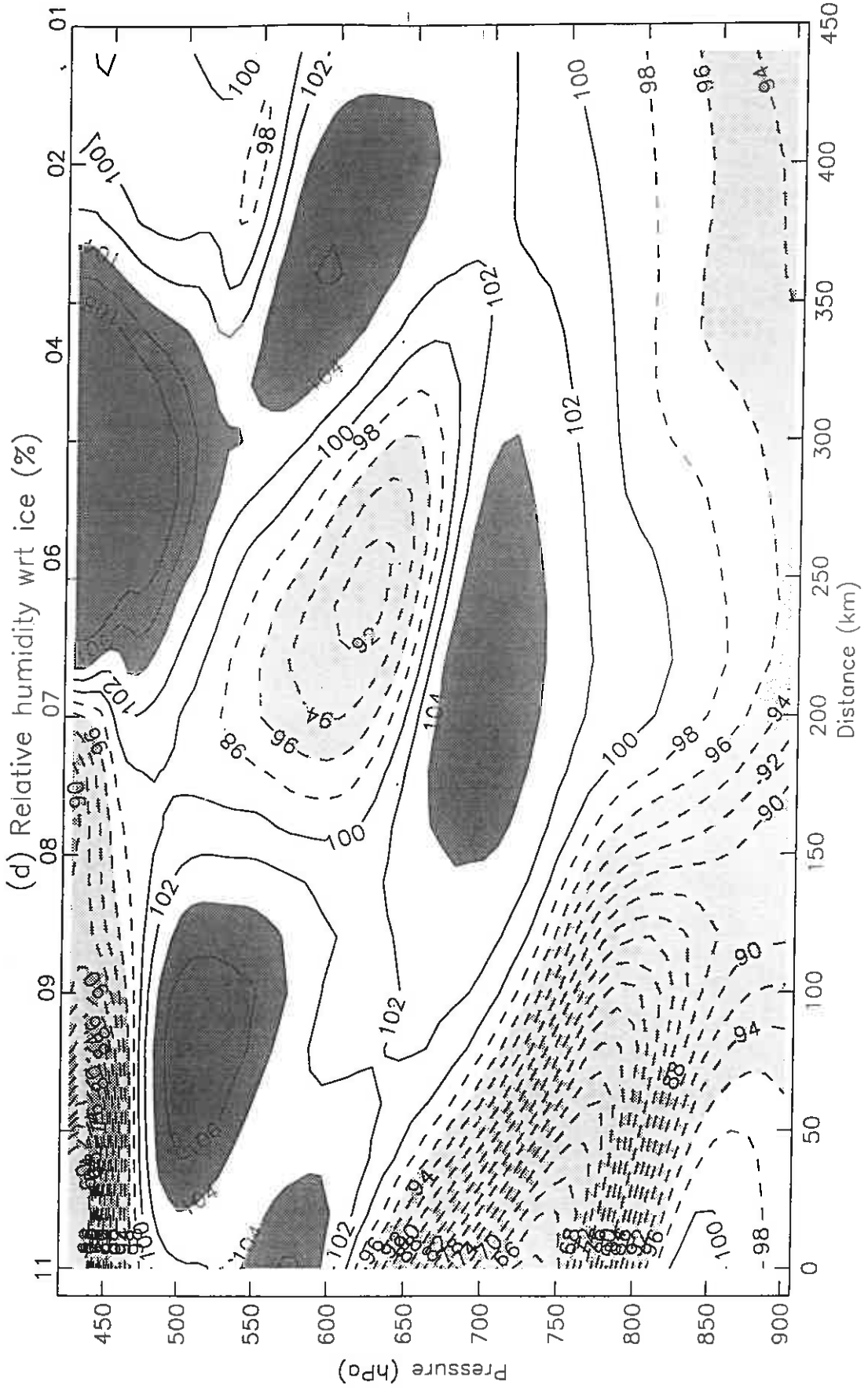
(d) Relative humidity wrt ice (%)
Pressure (hPa)
Distance (km)
450
500
550
600
650
700
750
800
850
900
0
50
100
150
200
250
300
350
400
450
01
02
04
06
07
08
09
11

Figure 5d

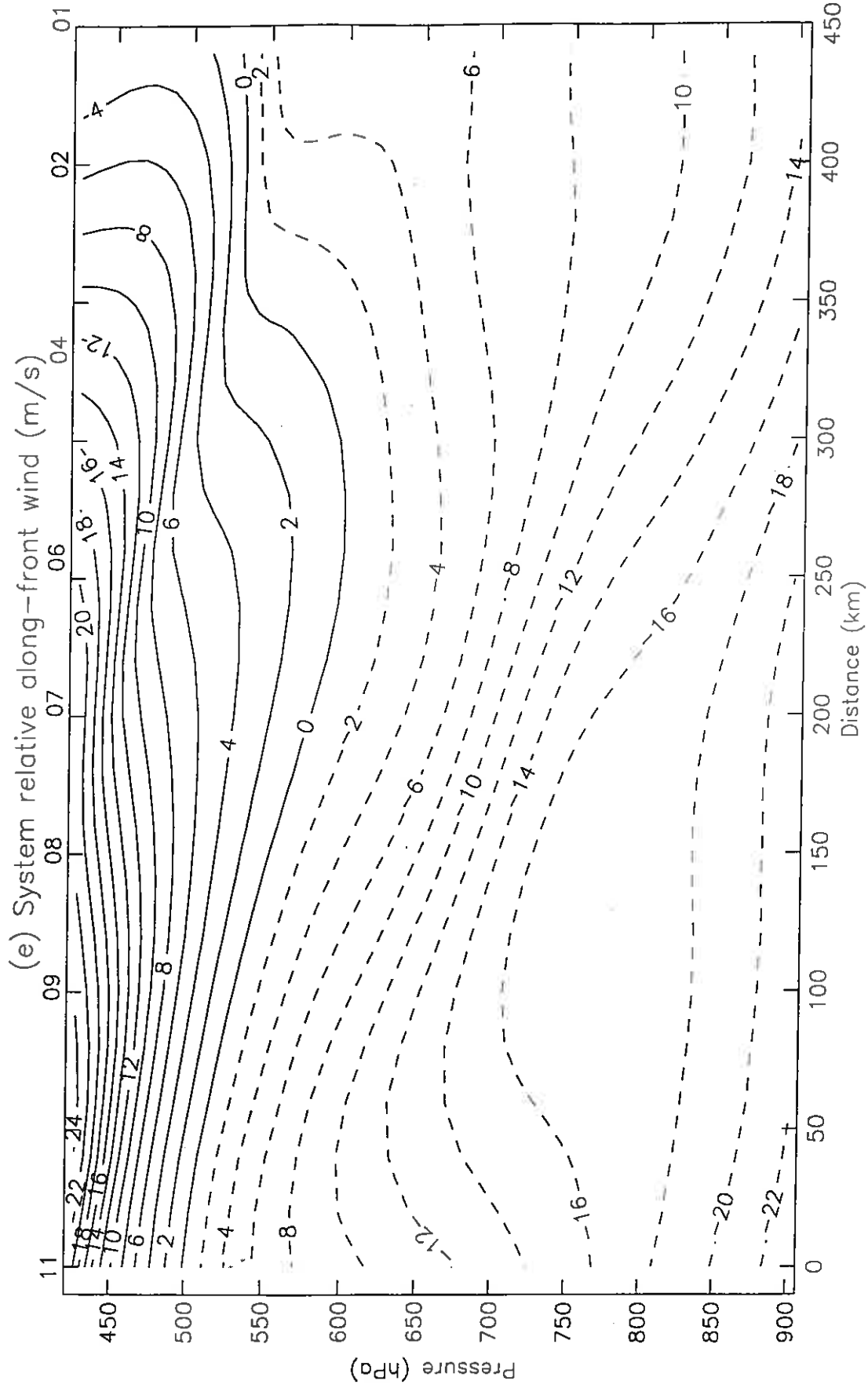
(e) System relative along-front wind (m/s)
Pressure (hPa)
Distance (km)
01
02
04
06
07
08
09
11
450
500
550
600
650
700
750
800
850
900
0
50
100
150
200
250
300
350
400
450

Figure 5e

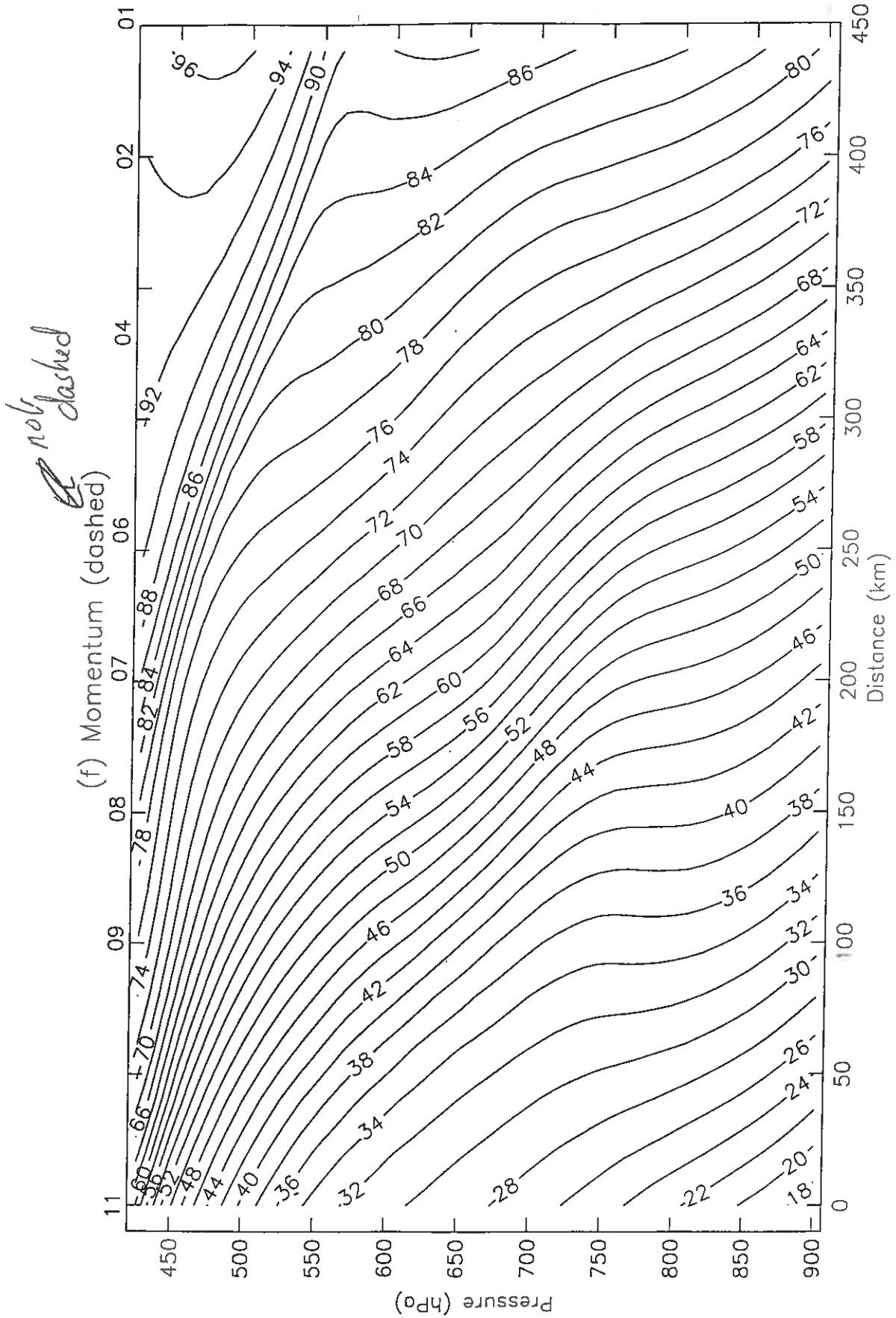
(f) Momentum (dashed)
not dashed
Pressure (hPa)
Distance (km)
450
500
550
600
650
700
750
800
850
900
0
50
100
150
200
250
300
350
400
450
01
02
04
06
07
08
09
11

Figure 5f

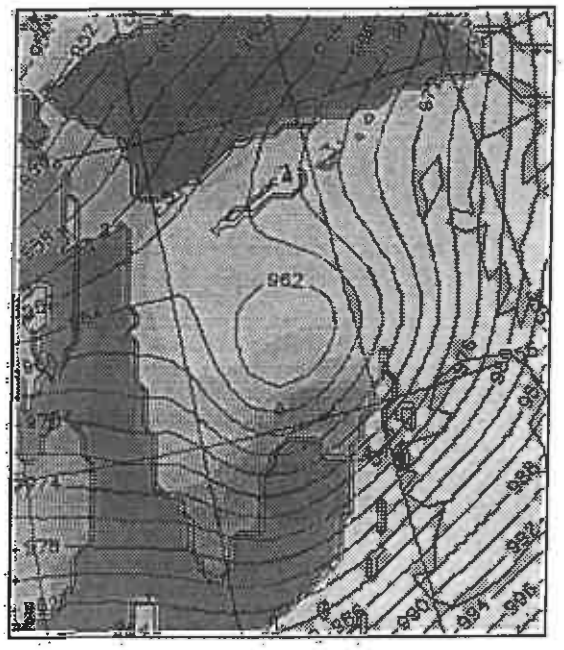

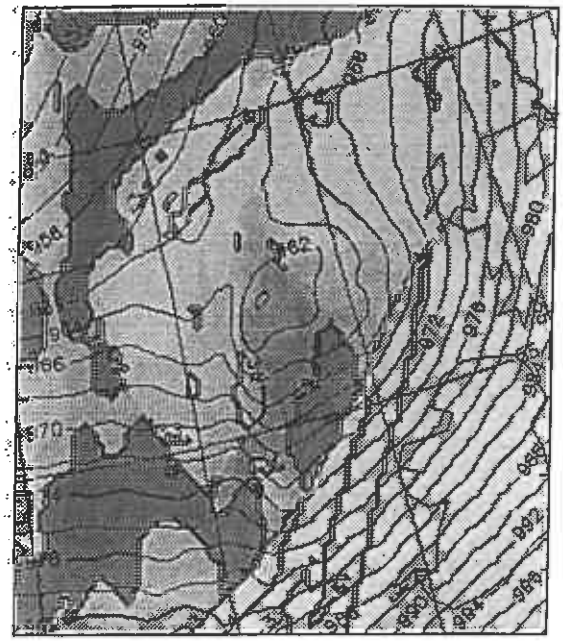

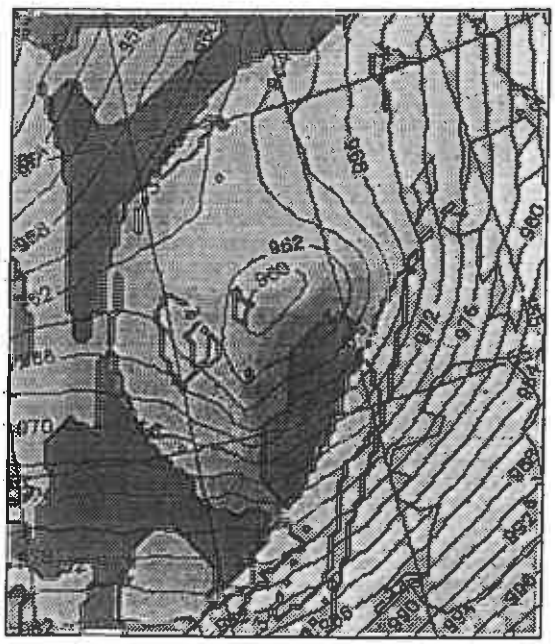

Figure 6

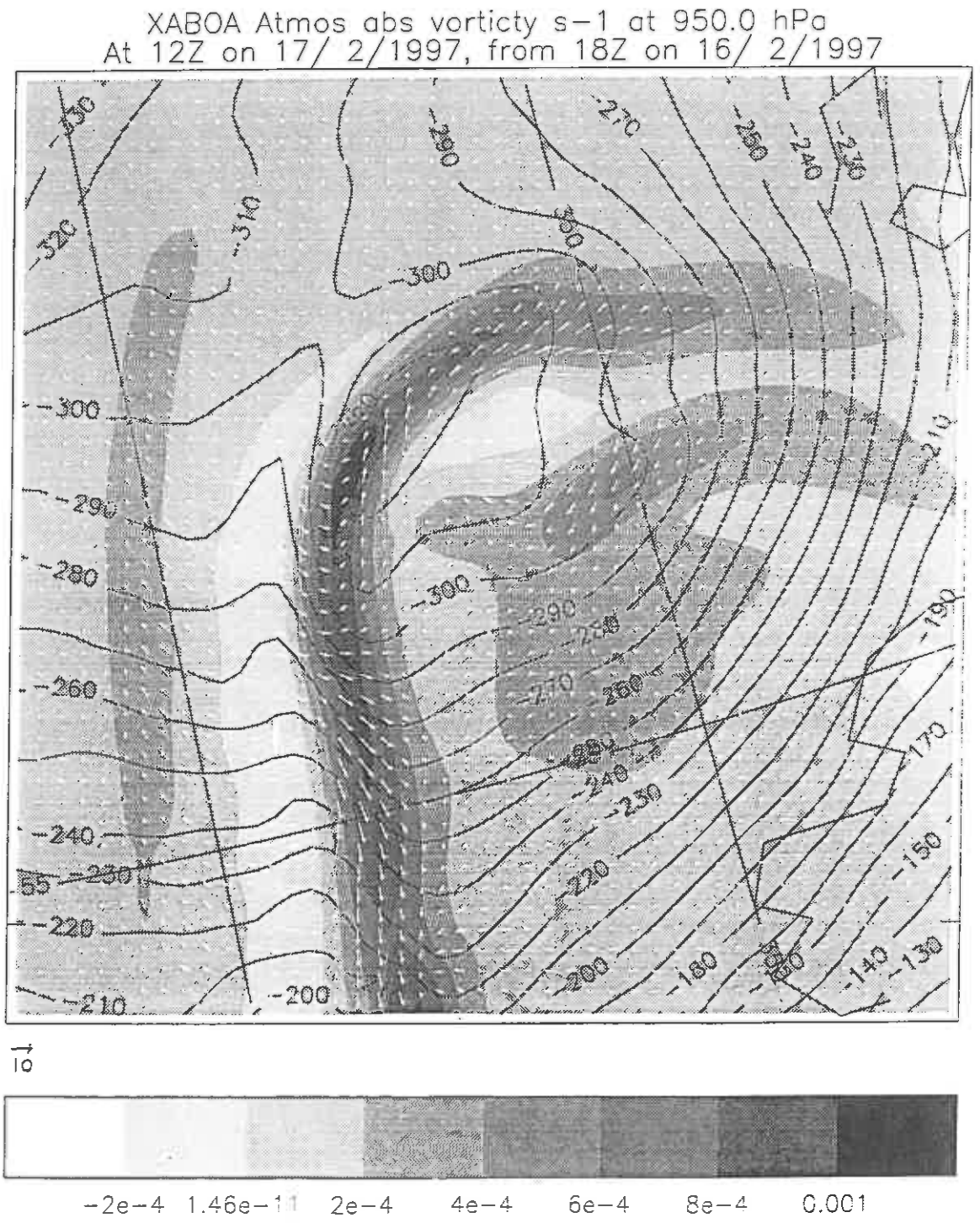
XABOA Atmos abs vorticty s-1 at 950.0 hPa
At 12Z on 17/ 2/1997, from 18Z on 16/ 2/1997
-2e-4
1.46e-11
2e-4
4e-4
6e-4
8e-4
0.001

Figure 7

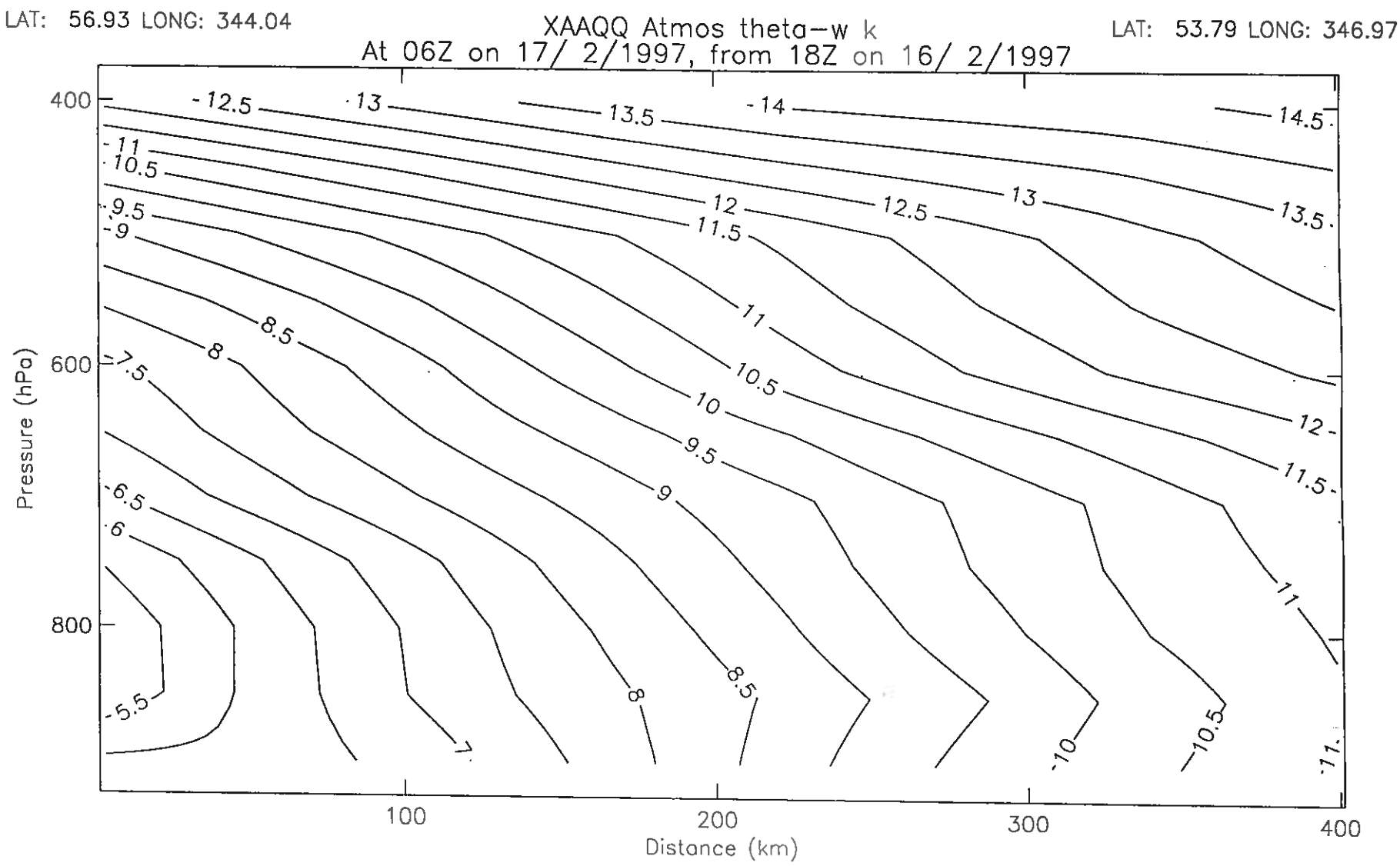
LAT: 56.93 LONG: 344.04
XAAQQ Atmos theta-w k
At 06Z on 17/ 2/1997, from 18Z on 16/ 2/1997
LAT: 53.79 LONG: 346.97
Pressure (hPa)
400
600
800
100
200
300
400
Distance (km)
-12.5
-13
-13.5
-14
-14.5
-11
-10.5
-9.5
-9
-12
-11.5
-13
-13.5
-11
-10.5
-10
-9.5
-8.5
-8
-7.5
-12
-11.5
-11
-9
-8.5
-8
-6.5
-6
-5.5
-7
-10
-10.5
-11

Figure 8a

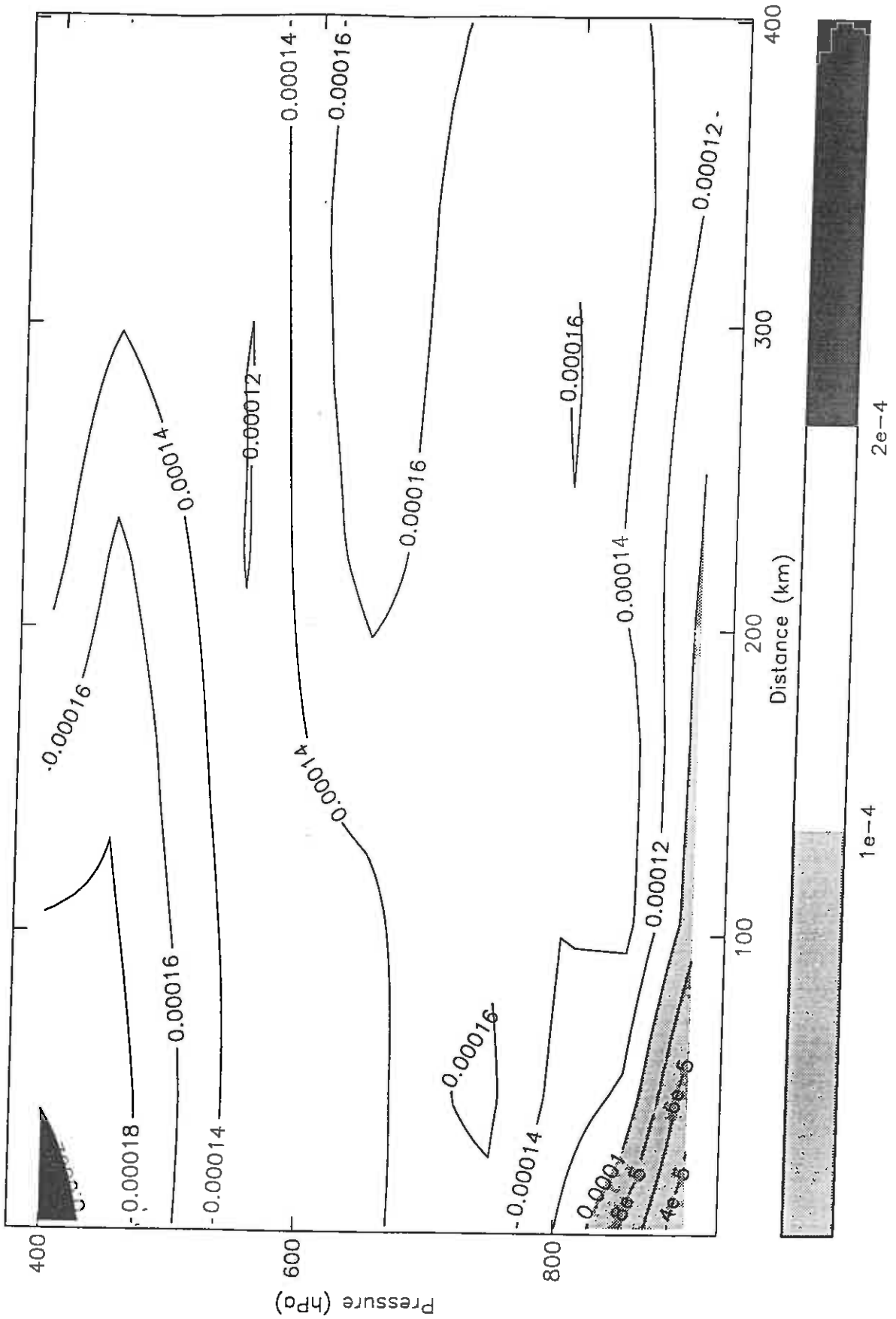
Pressure (hPa)
400
600
800
100
200
300
400
Distance (km)
1e-4
2e-4
0.00012
0.00014
0.00016
0.00018

Figure 8b

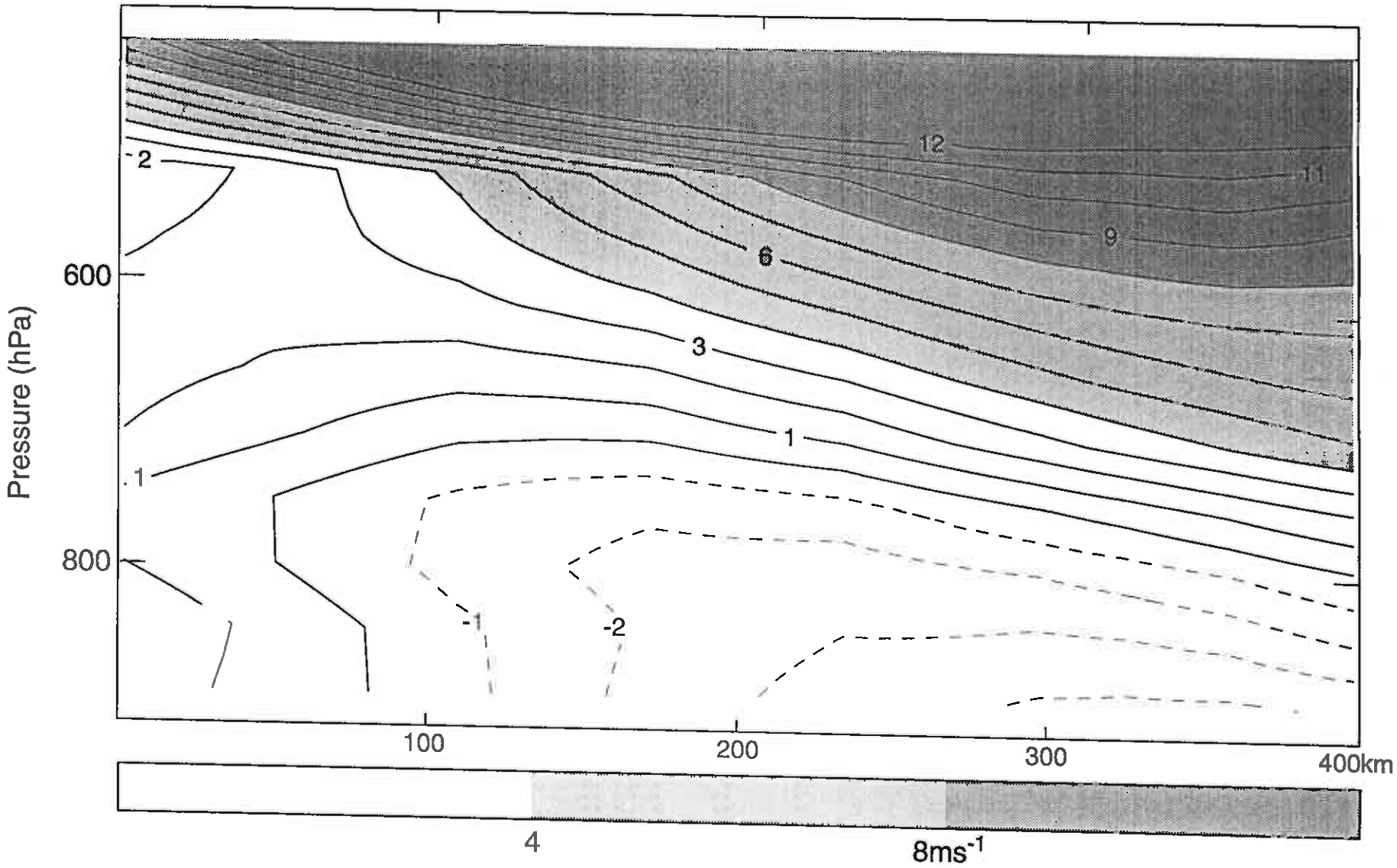

Figure 8c

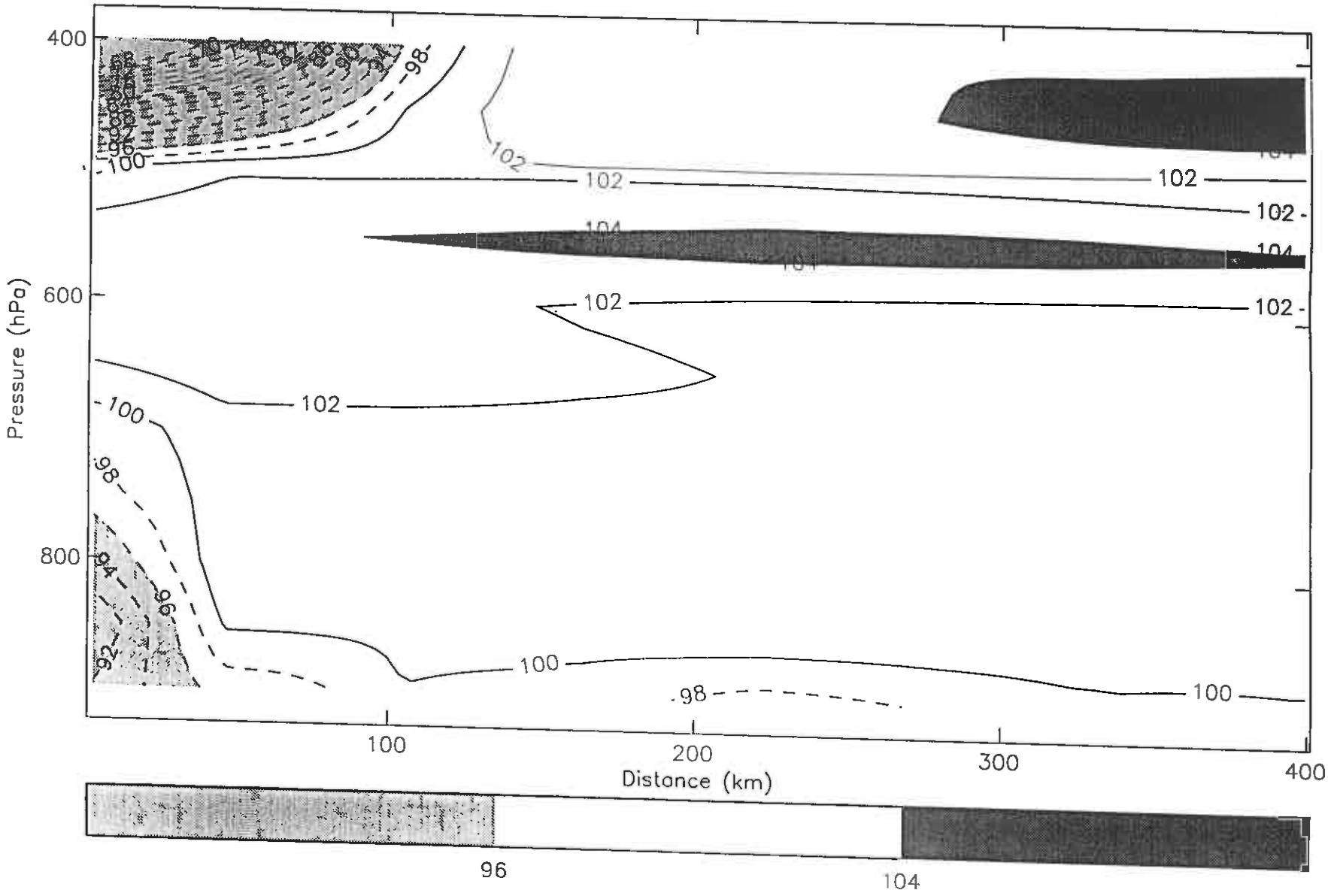
400
600
800
Pressure (hPa)
98
100
102
102
102
104
102
102
100
98
96
94
92
100
98
100
100
100
200
300
400
Distance (km)
96
104

Figure 8d

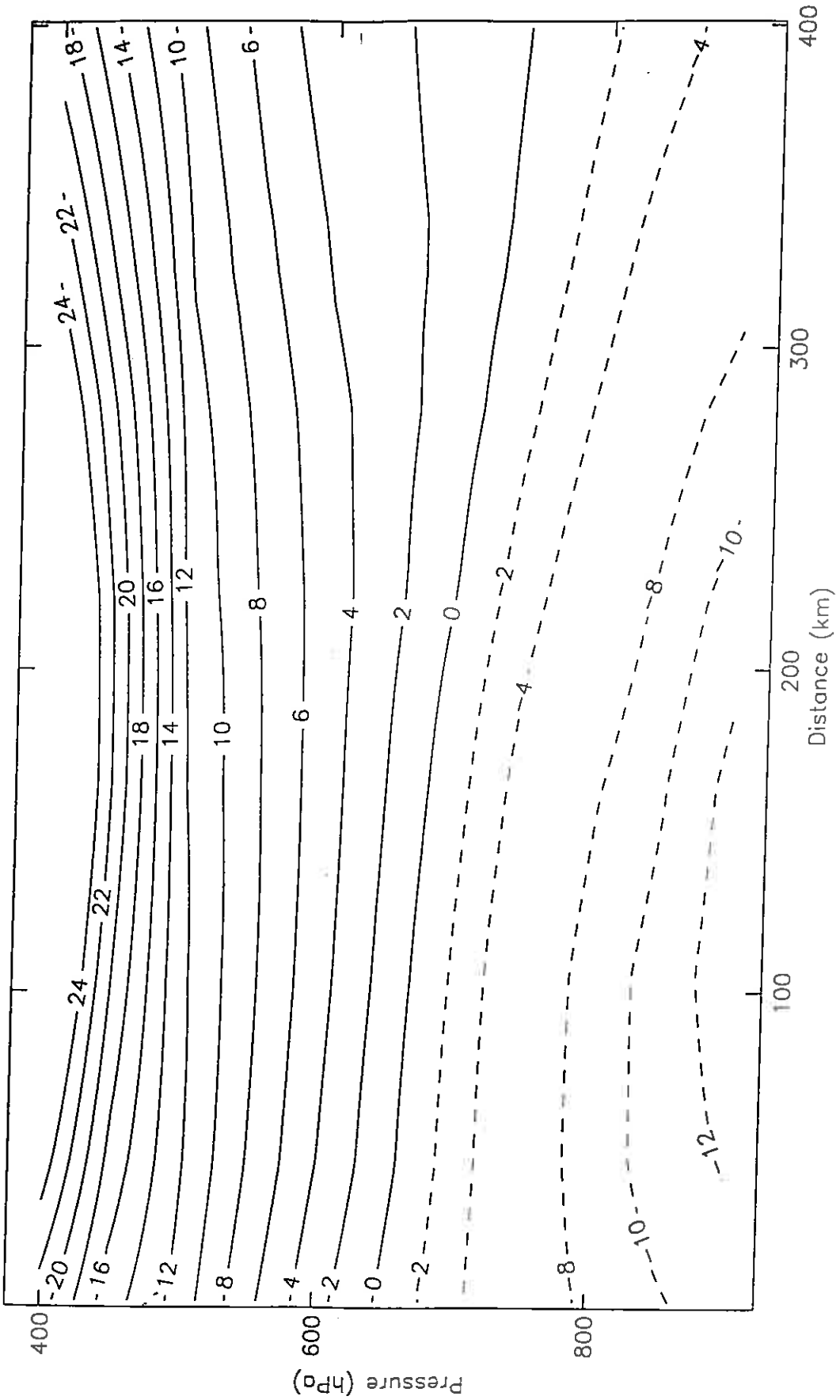
Pressure (hPa)
400
600
800
100
200
300
400
Distance (km)
-20
-16
-12
-8
-4
-0
24
22
20
18
16
14
12
10
8
6
4
2
0
-2
-4
-8
-10
-12

Figure 8e

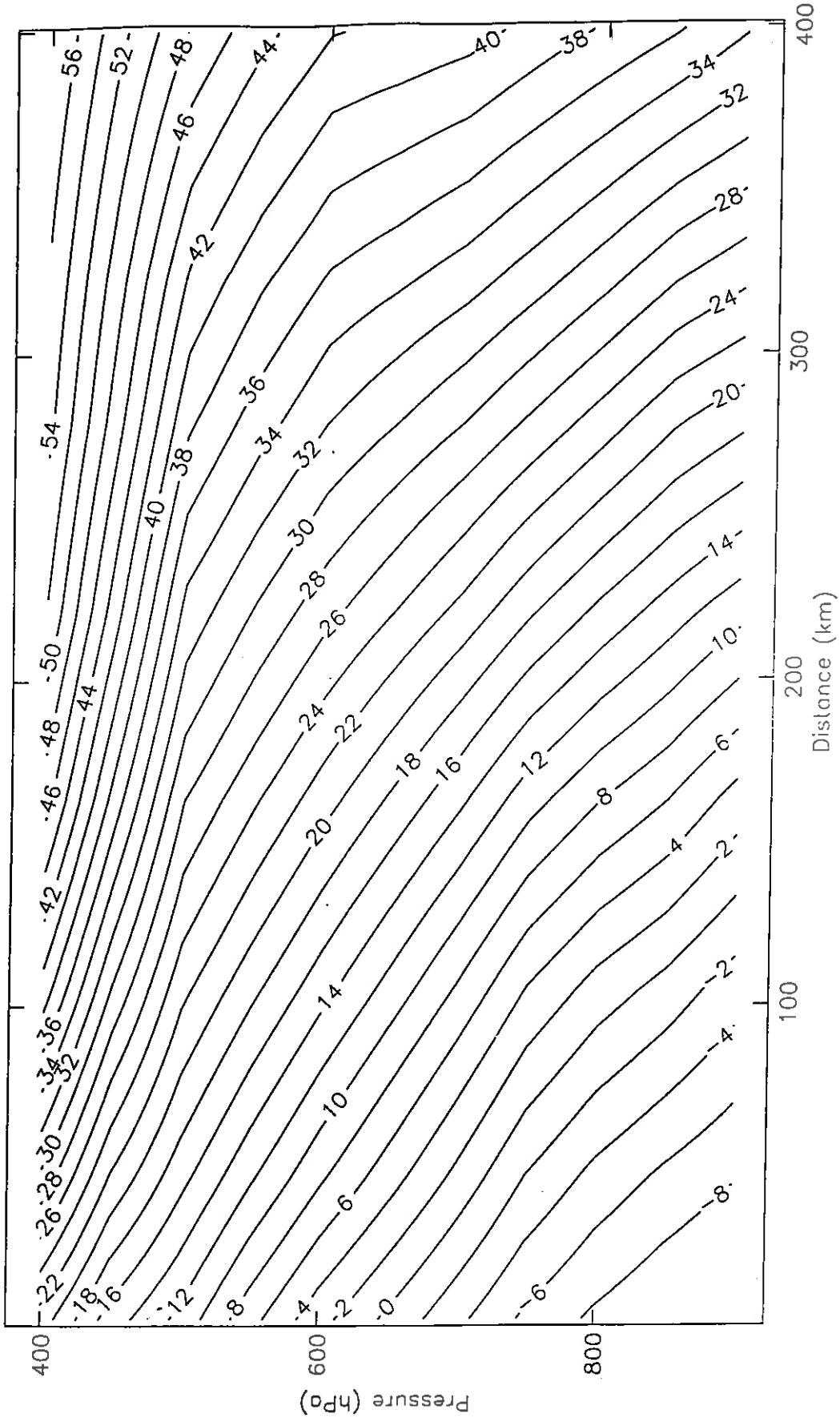

Figure 8f

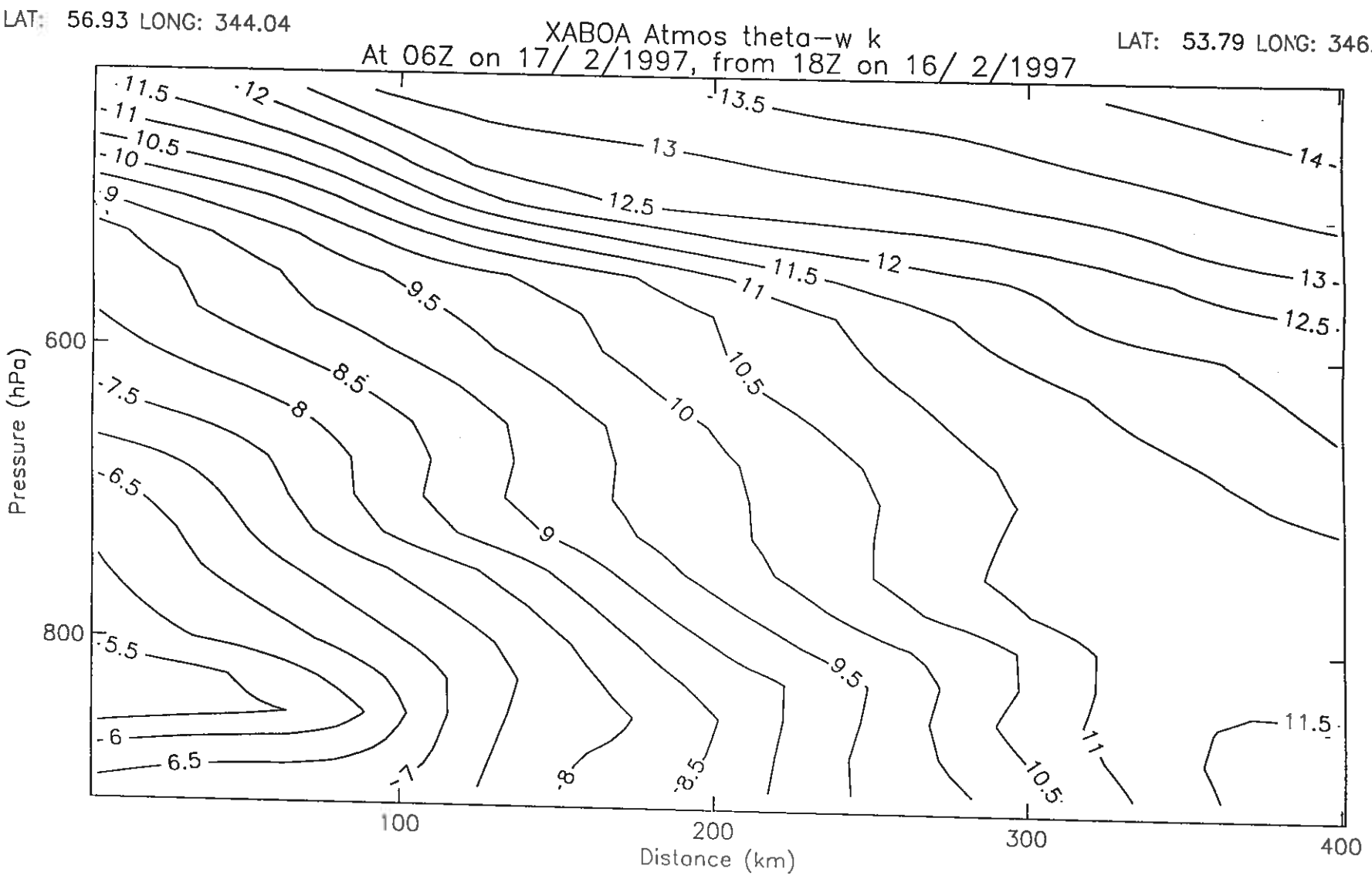
LAT: 56.93 LONG: 344.04
XABOA Atmos theta–w k
At 06Z on 17/ 2/1997, from 18Z on 16/ 2/1997
LAT: 53.79 LONG: 346.97
Pressure (hPa)
600
800
100
200
300
400
Distance (km)
11.5
12
13.5
13
14
12.5
11
10.5
10
9
9.5
8.5
8
7.5
6.5
6
5.5
7
8
8.5
9
9.5
10
10.5
11
11.5
12
13
12.5
10.5

Figure 9a

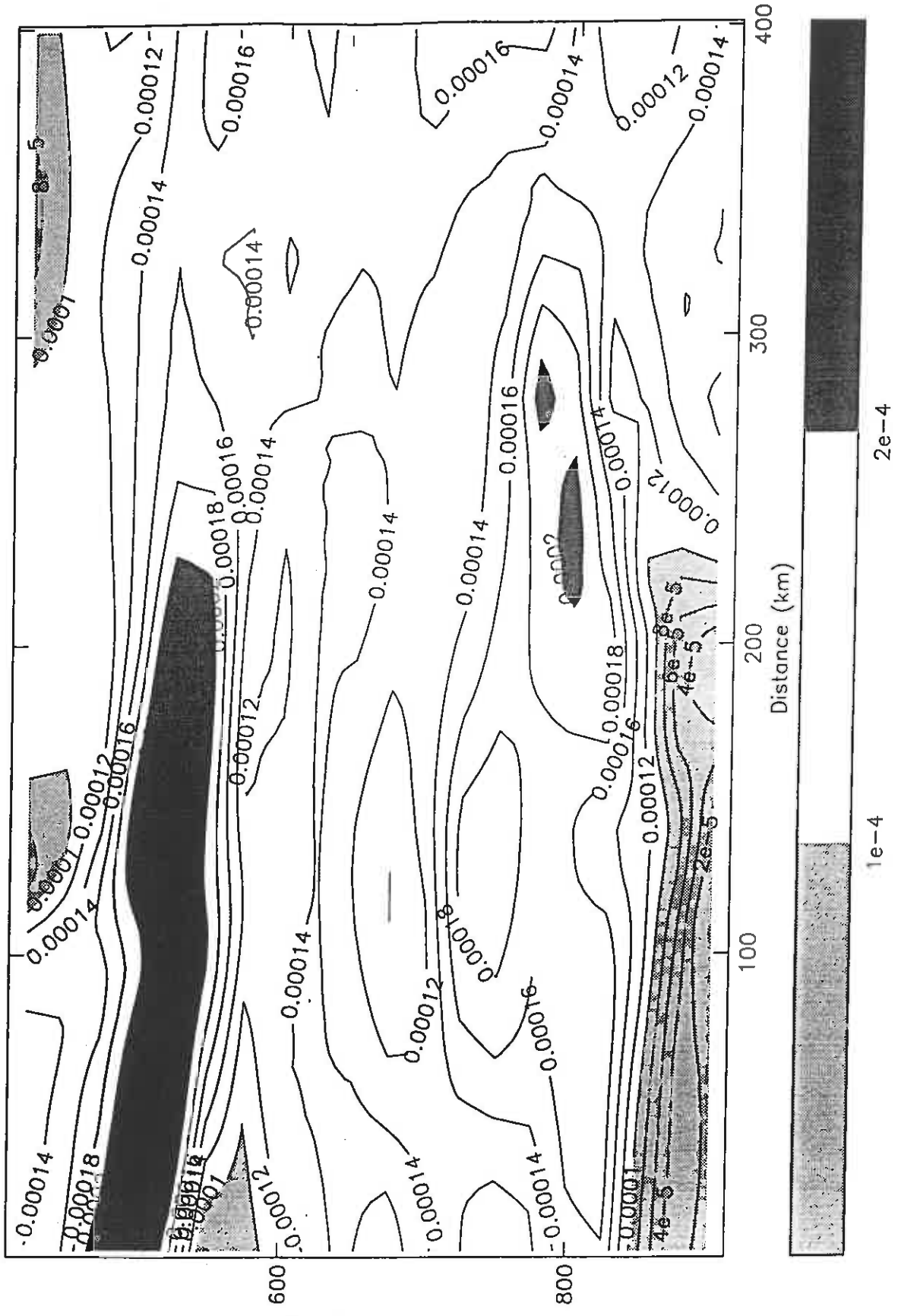

Figure 9b

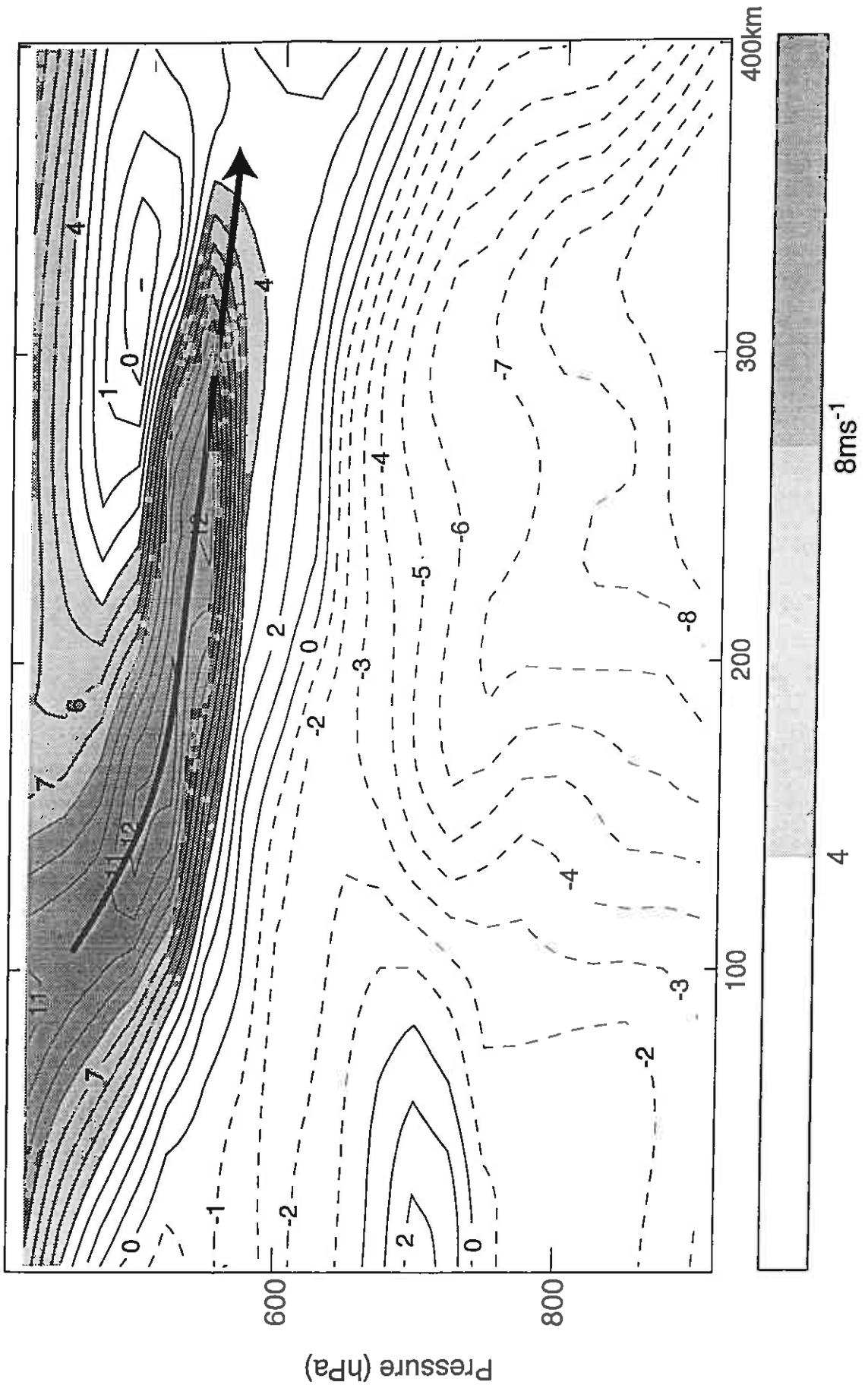

Figure 9c

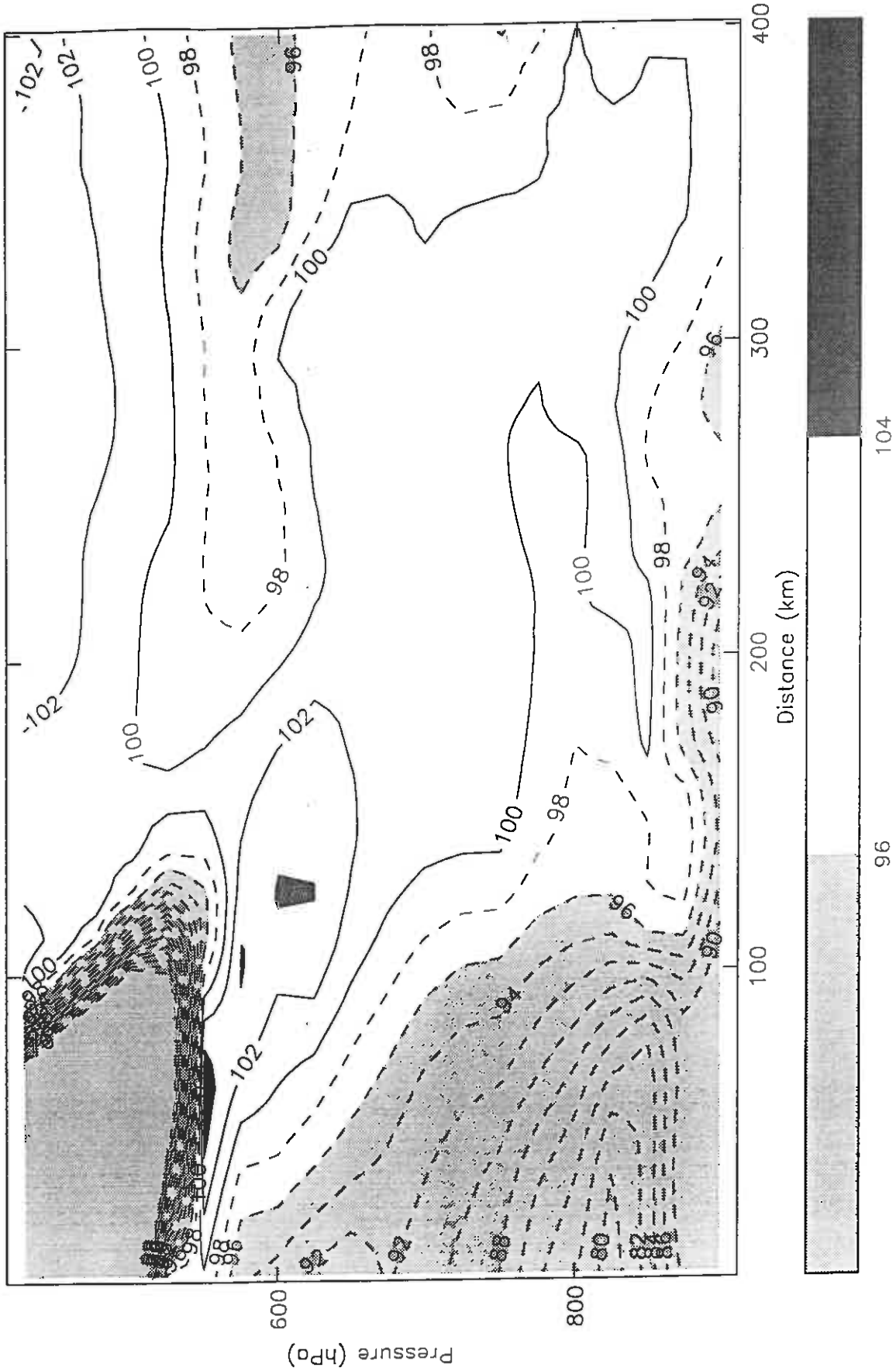

Figure 9d

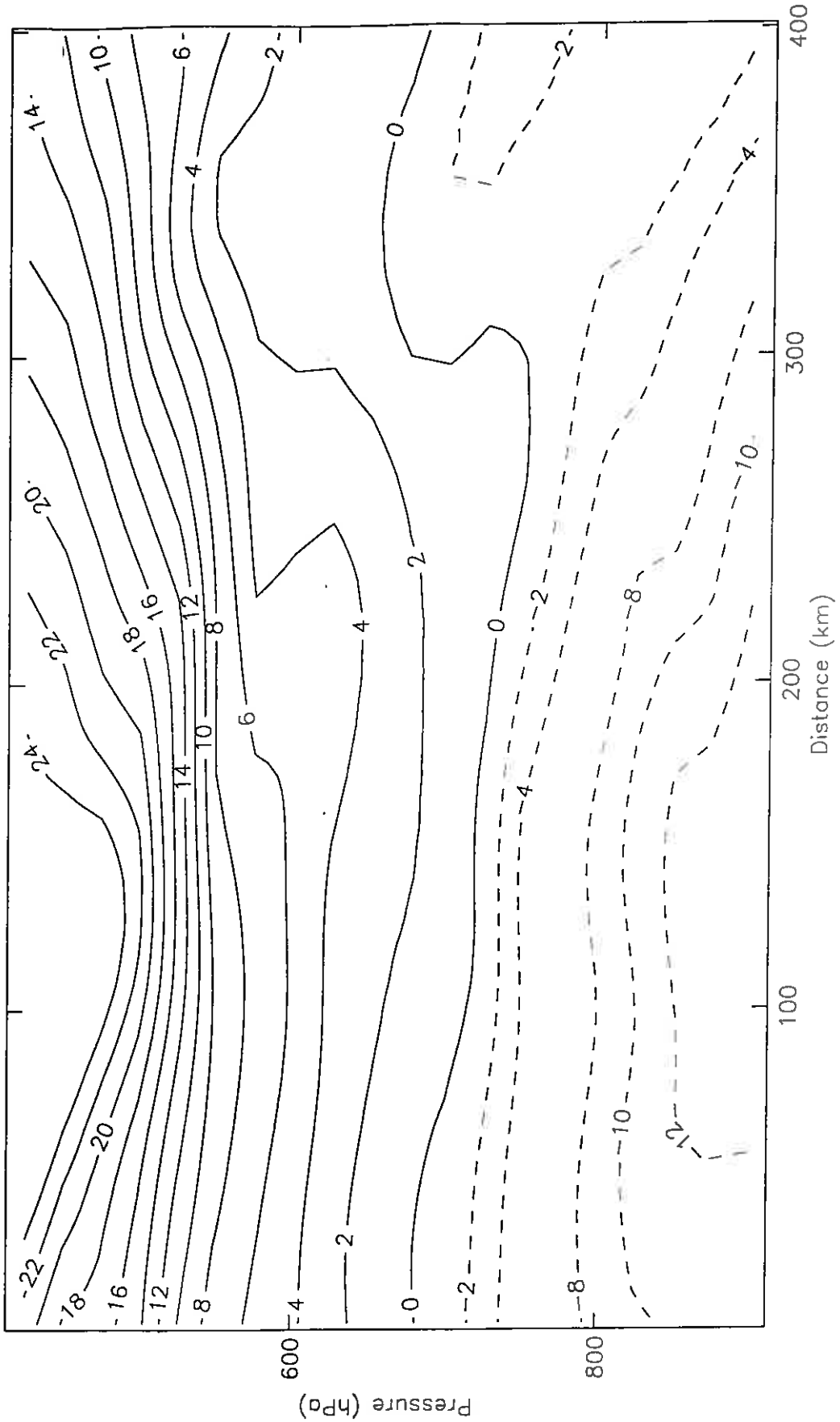

Figure 9e

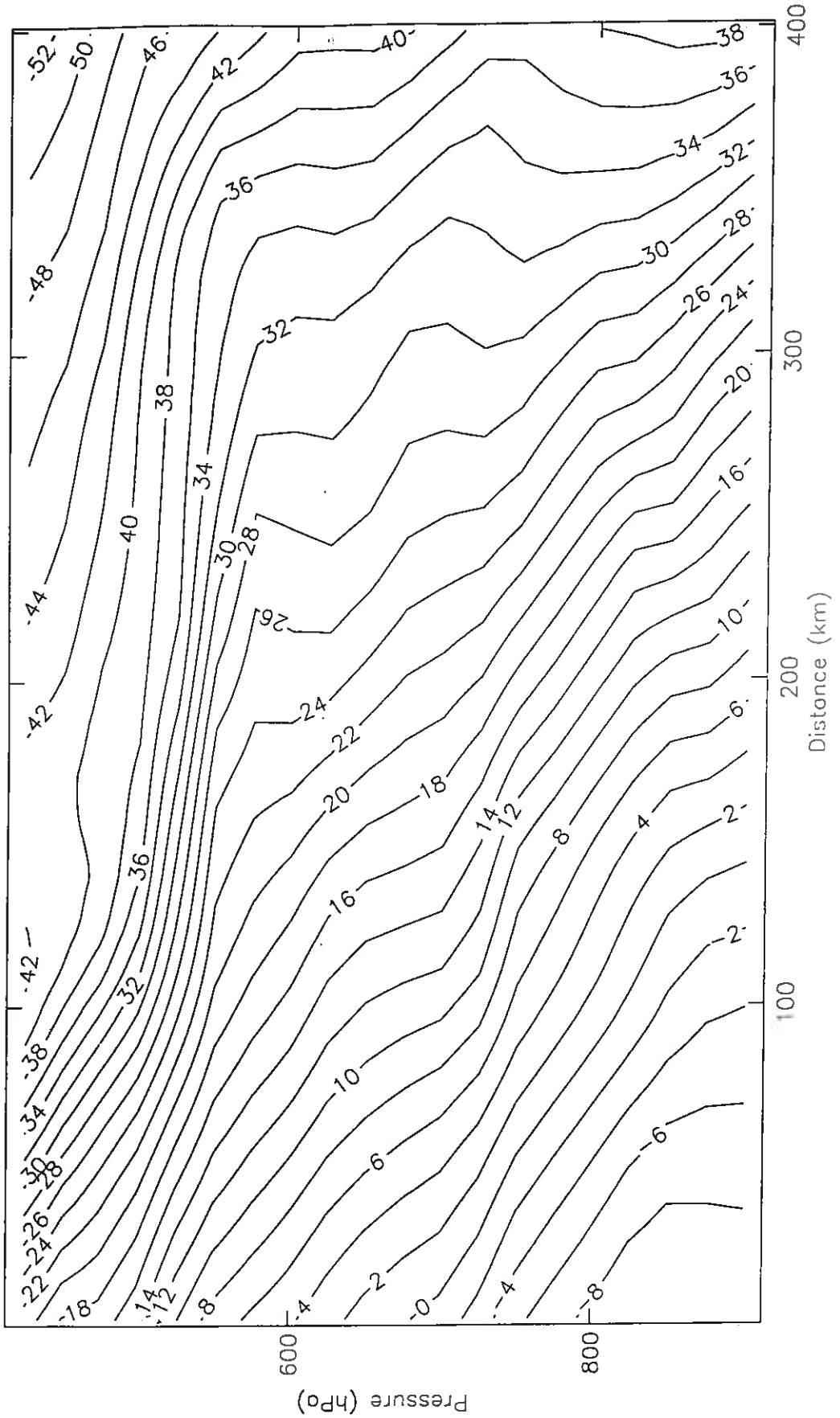

Figure 9f

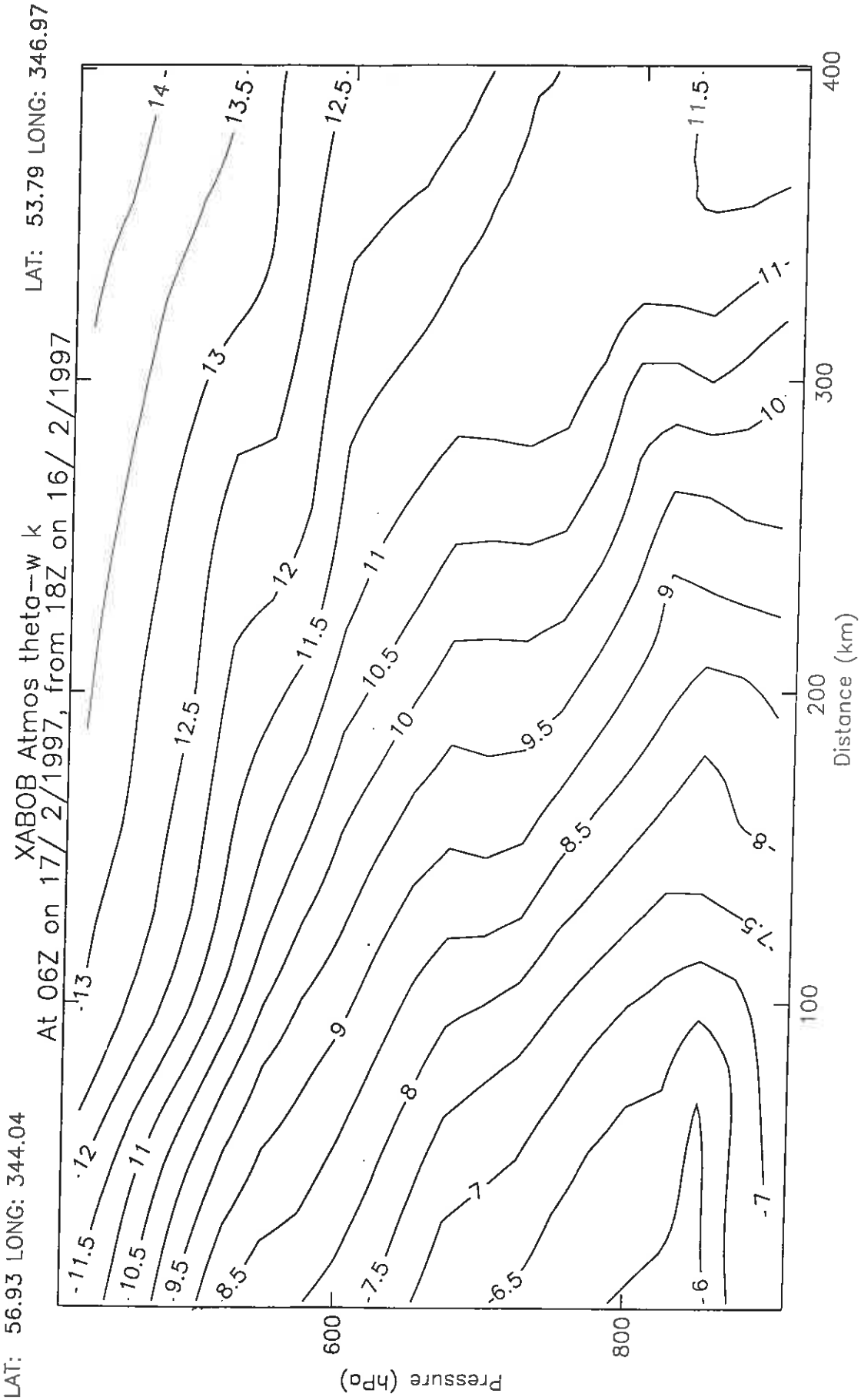
XABOB Atmos theta–w k
At 06Z on 17/ 2/1997, from 18Z on 16/ 2/1997
LAT: 56.93 LONG: 344.04
LAT: 53.79 LONG: 346.97
Pressure (hPa)
Distance (km)
600
800
100
200
300
400
14
13.5
13
12.5
12
11.5
11
10.5
10
9.5
9
8.5
8
7.5
7
6.5
6
11.5
11
10.5
10
9.5
9
8.5
8
7.5
7
6.5
6

Figure 10a

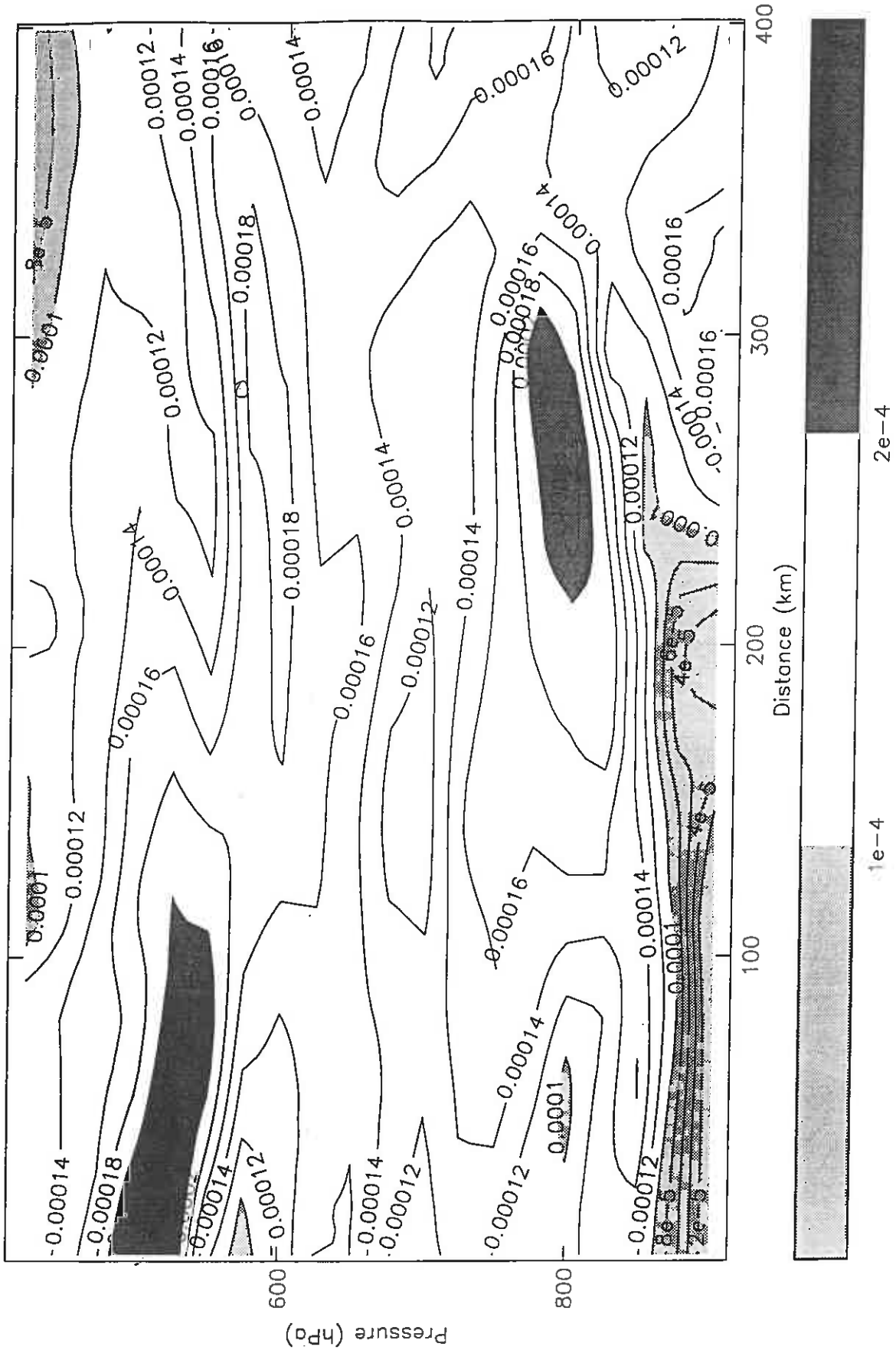

Figure 10b

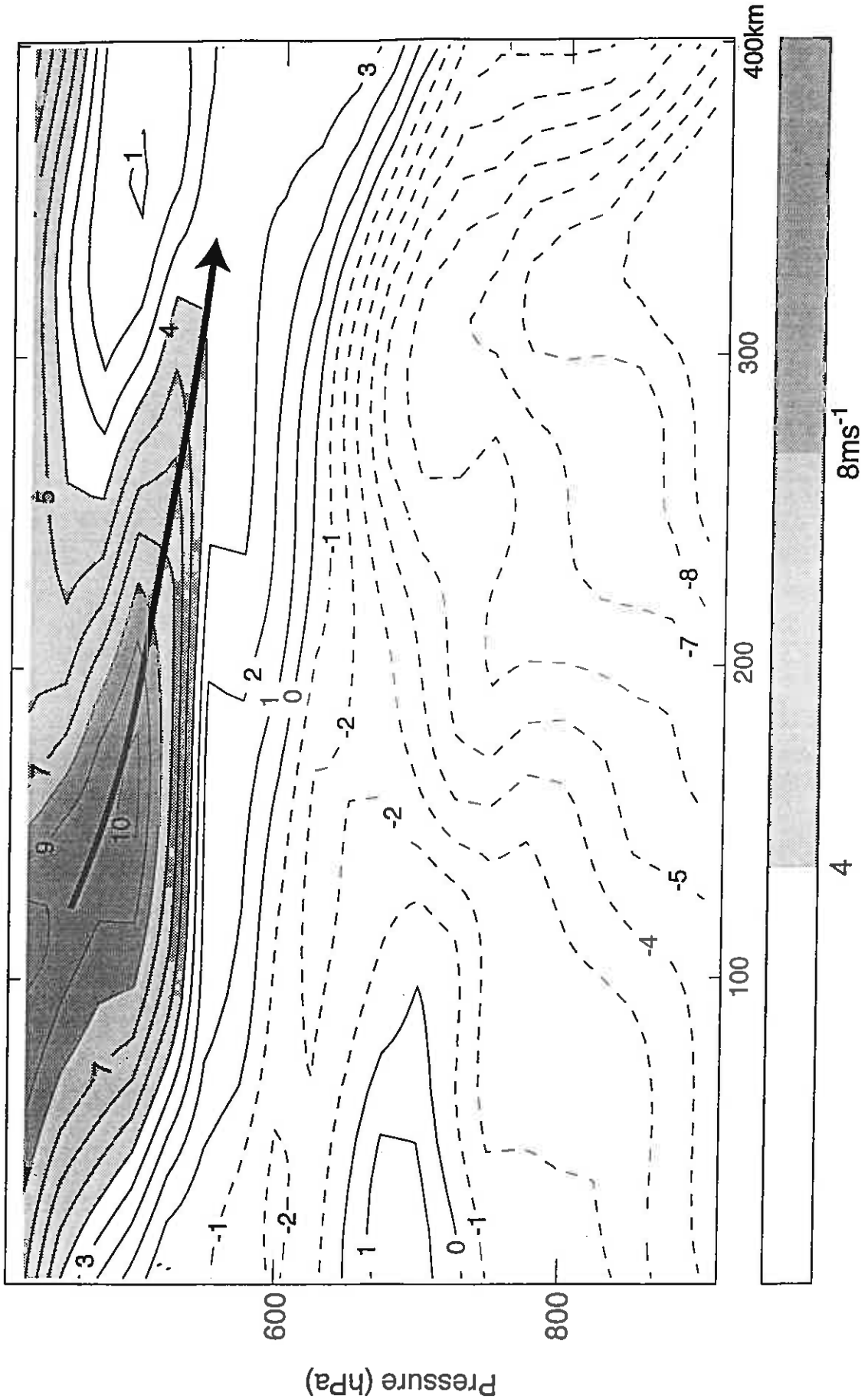

Figure 10c

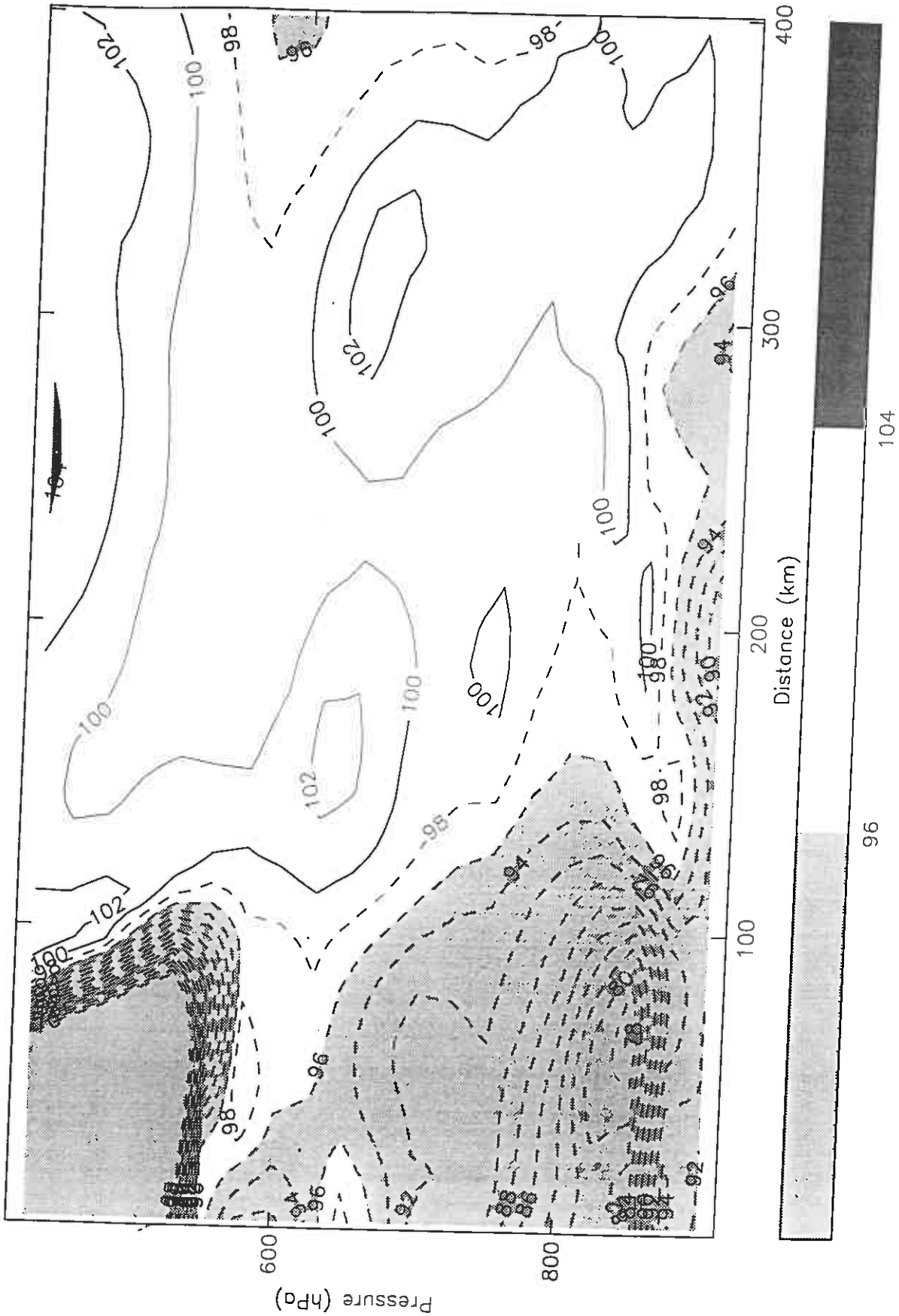

Figure 10d

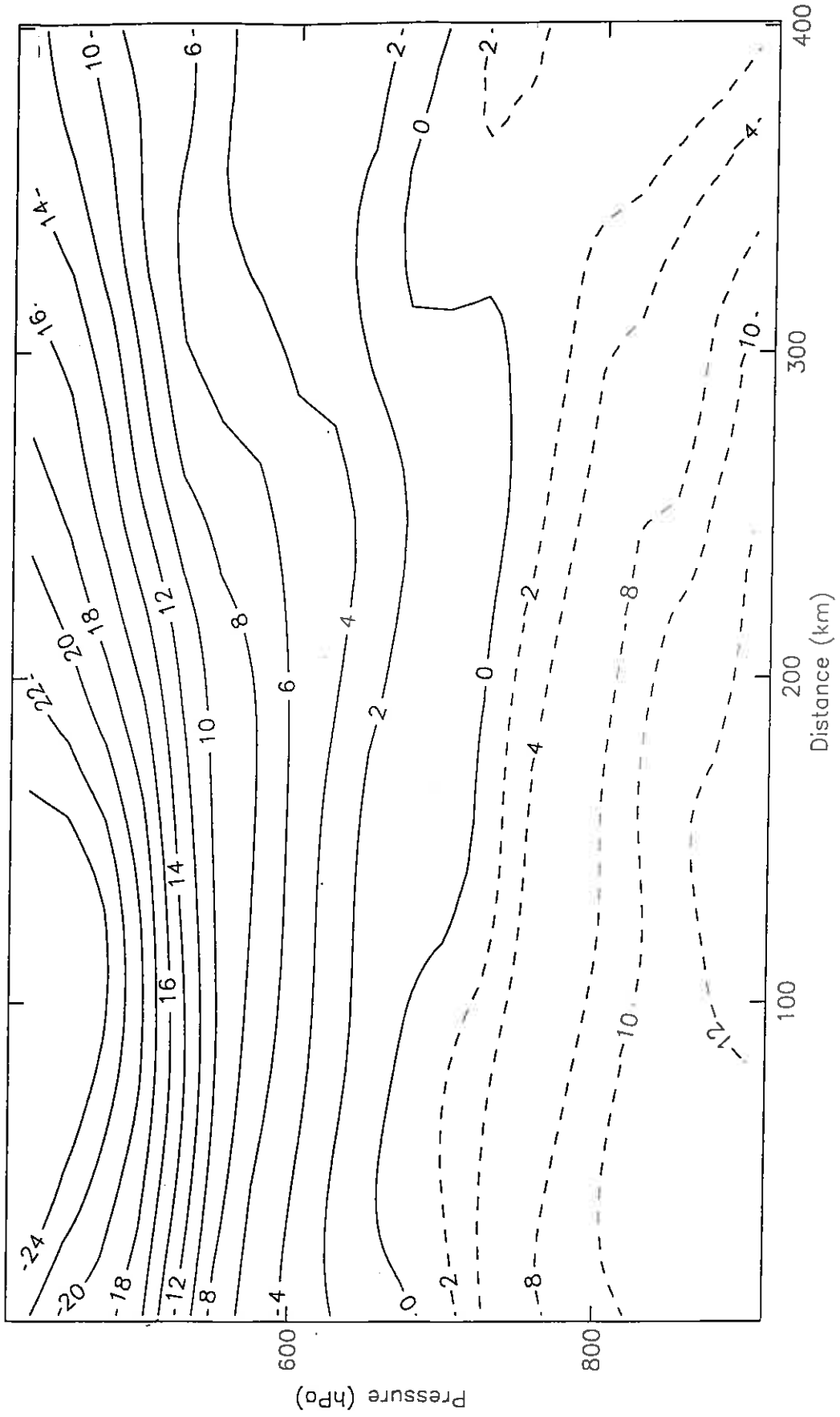

Figure 10e

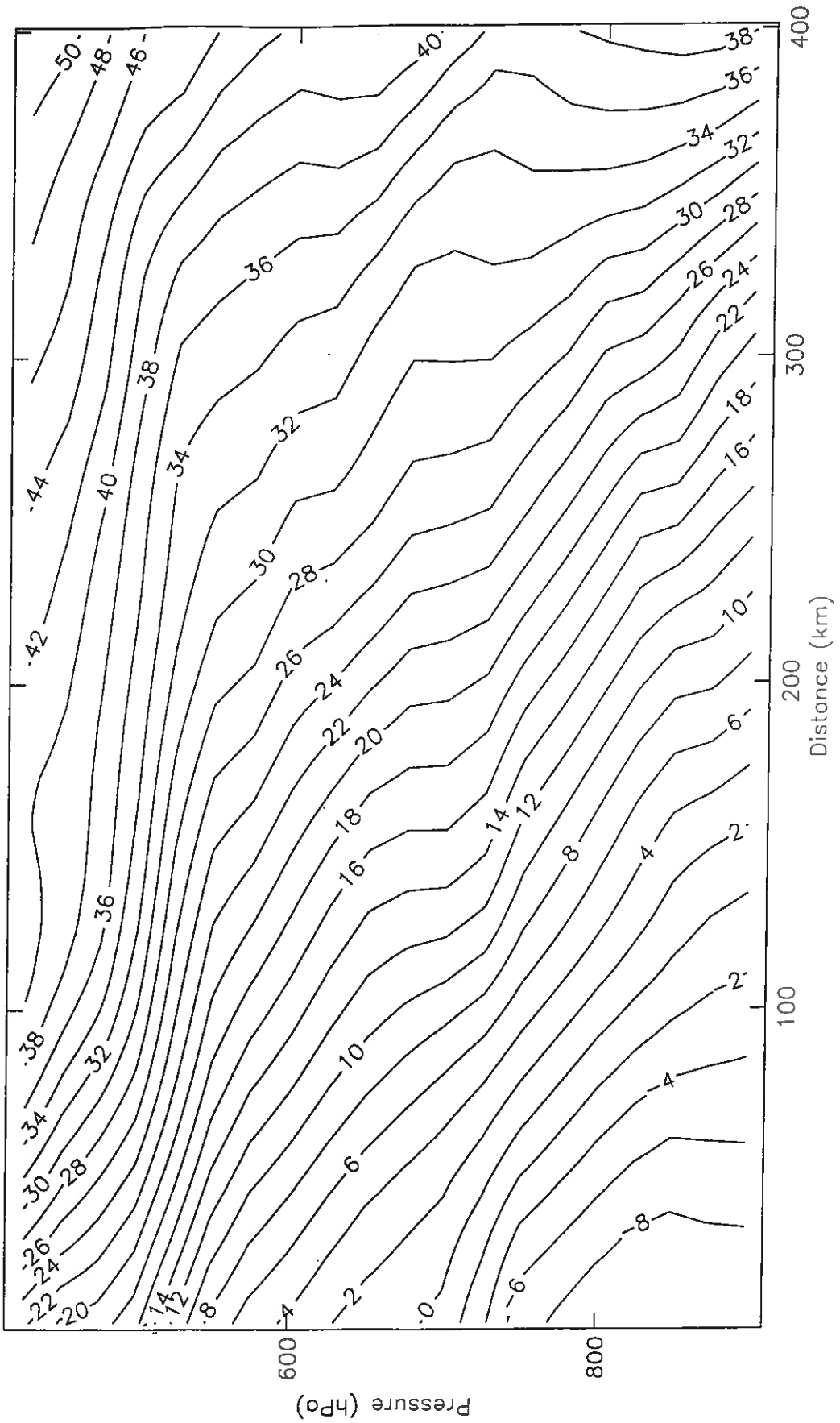

Figure 10f

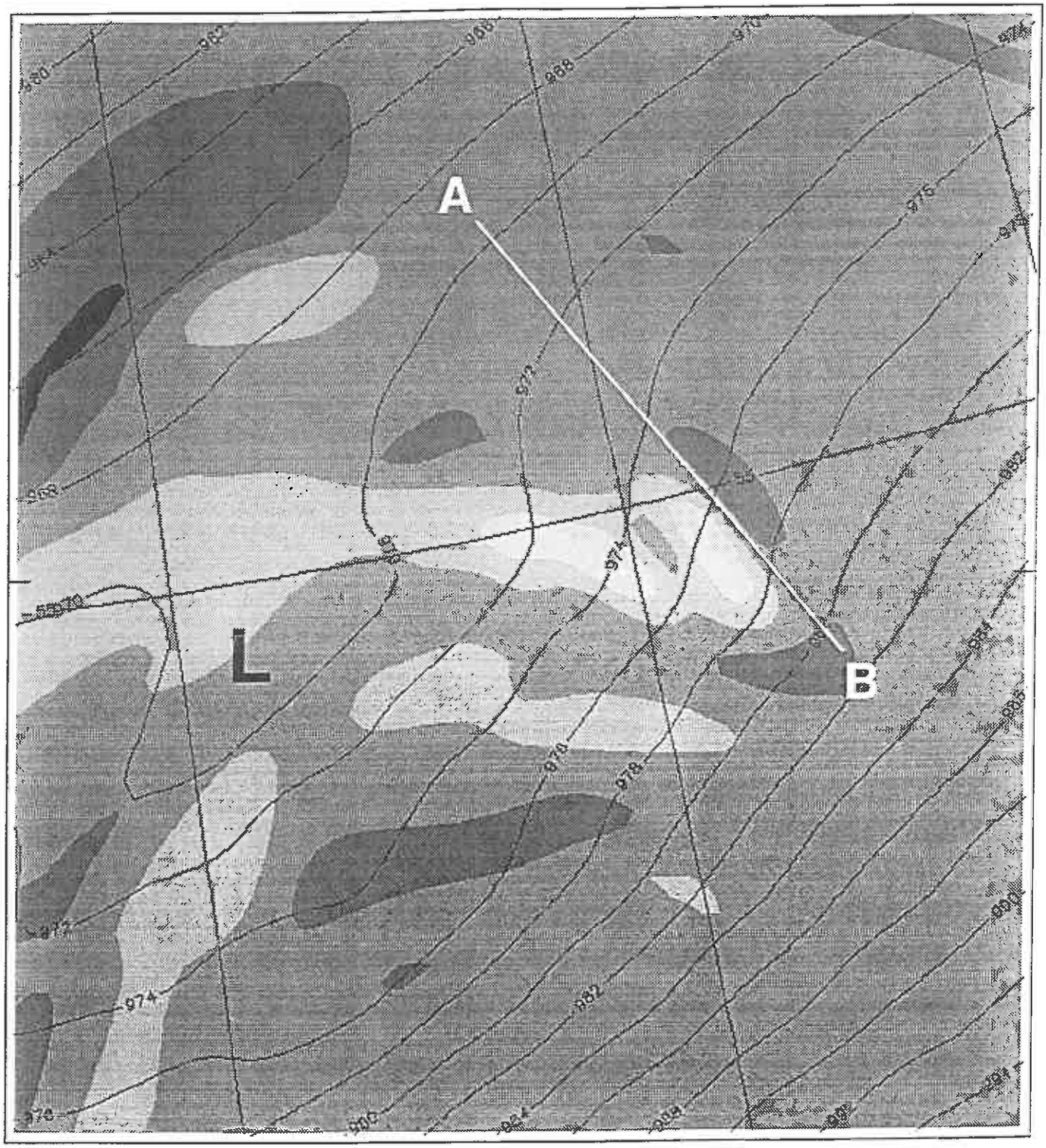

Figure 11

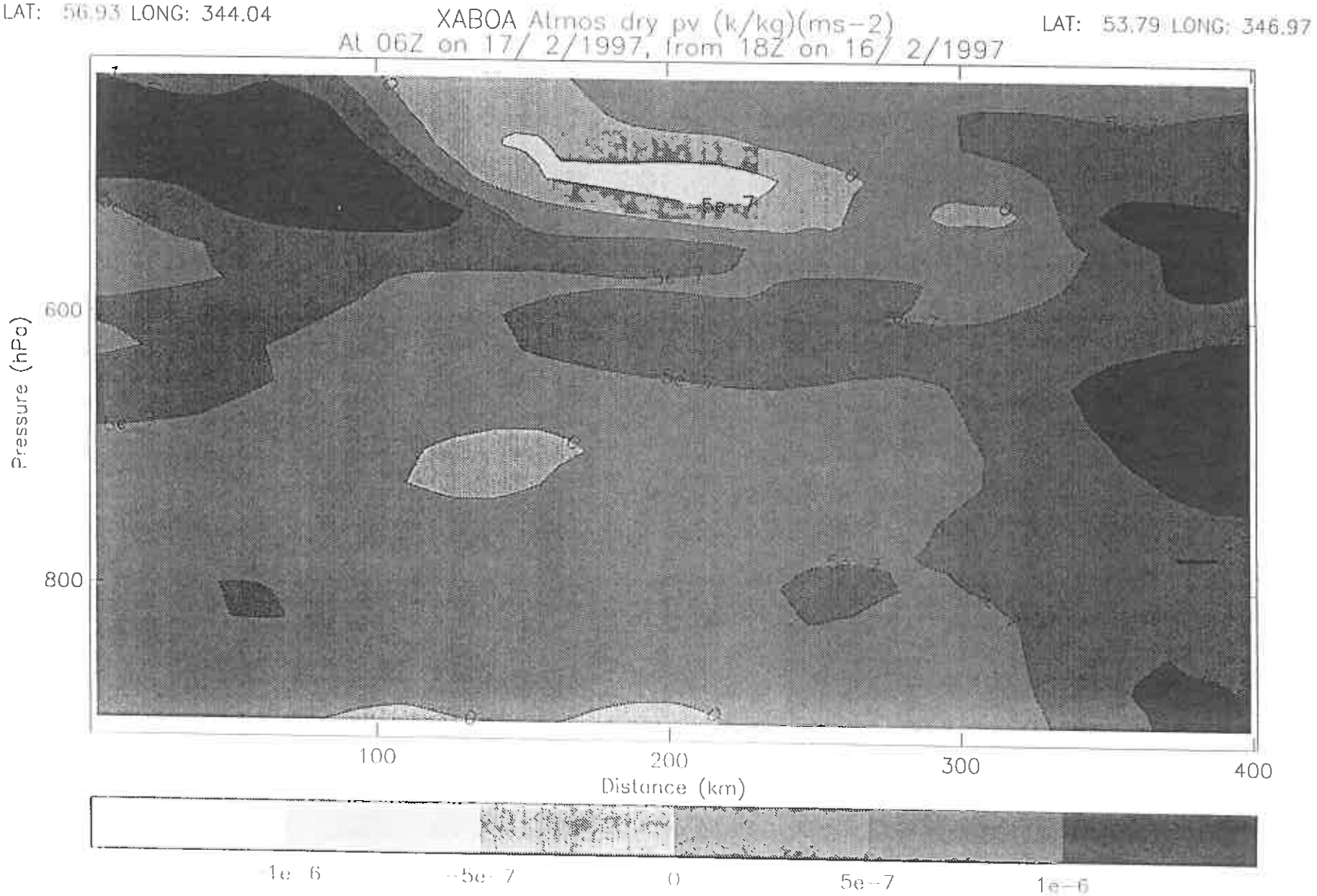
LAT: 56.93 LONG: 344.04
XABOA Atmos dry pv (k/kg)(ms-2)
At 06Z on 17/ 2/1997, from 18Z on 16/ 2/1997
LAT: 53.79 LONG: 346.97
Pressure (hPa)
600
800
100
200
300
400
Distance (km)
1e-6
-5e-7
0
5e-7
1e-6

Figure 12a

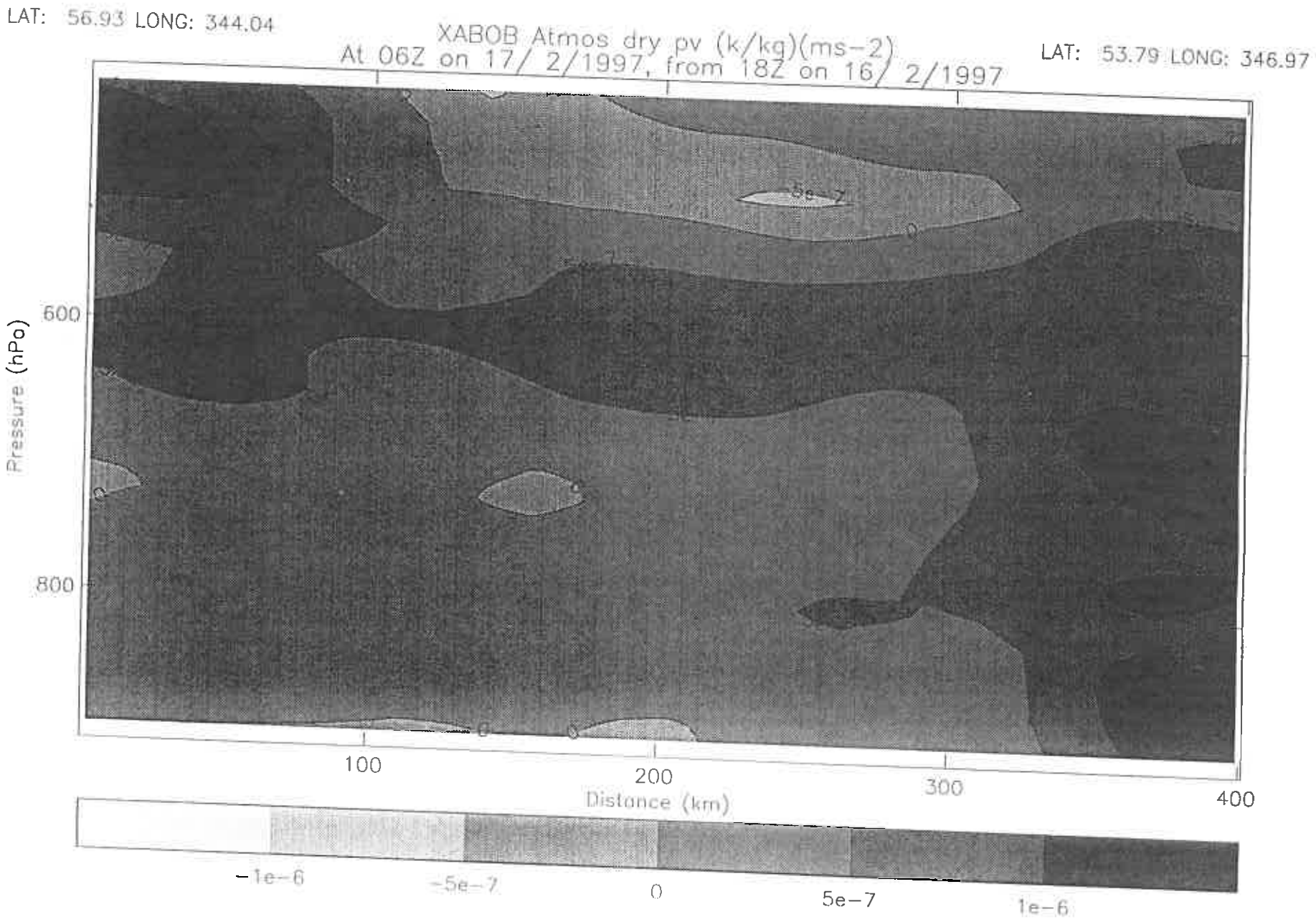
LAT: 56.93 LONG: 344.04
XABOB Atmos dry pv (k/kg)(ms-2)
At 06Z on 17/ 2/1997, from 18Z on 16/ 2/1997
LAT: 53.79 LONG: 346.97
Pressure (hPa)
600
800
100
200
300
400
Distance (km)
-1e-6
-5e-7
0
5e-7
1e-6

Figure 12b

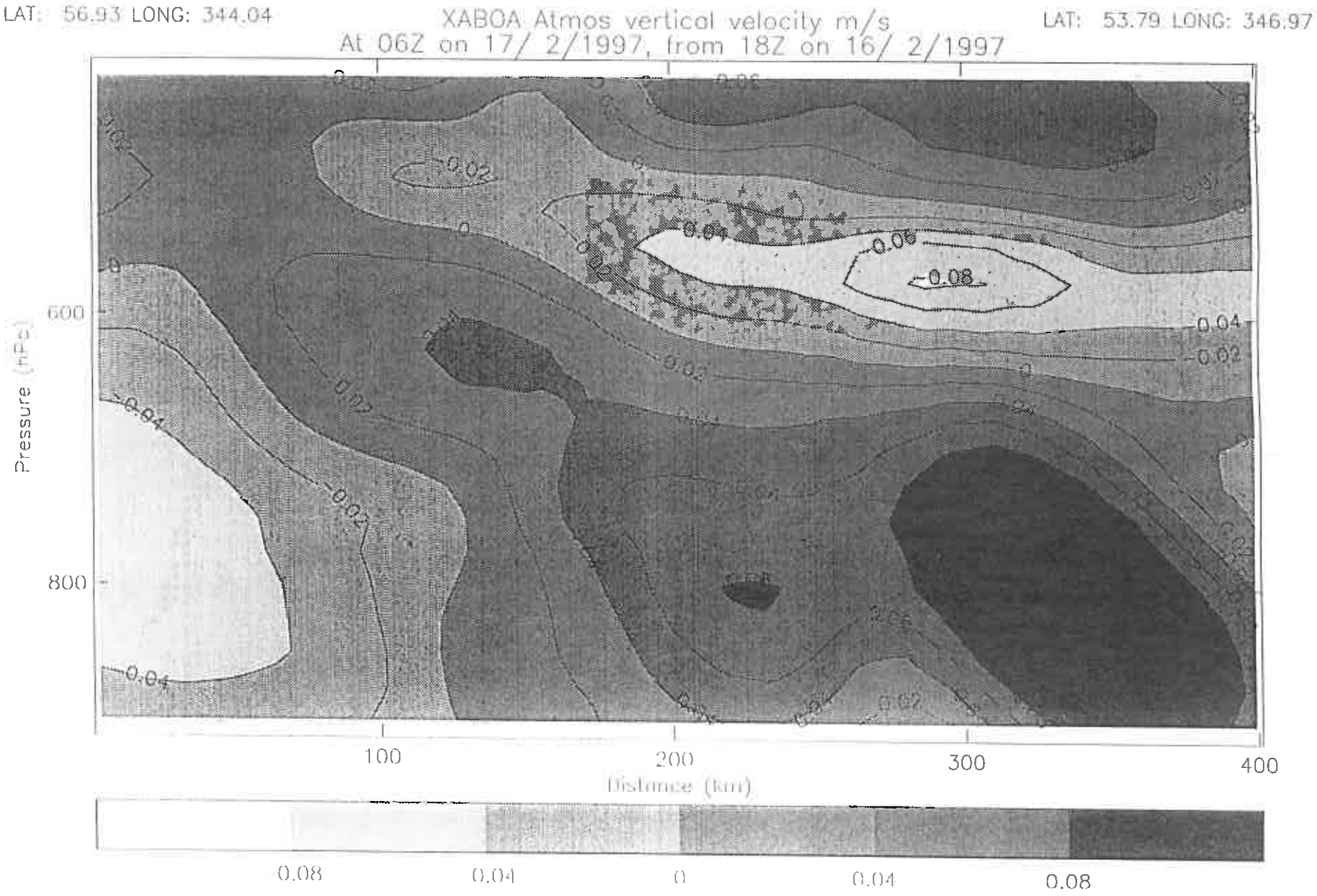
LAT: 56.93 LONG: 344.04
XABOA Atmos vertical velocity m/s
At 06Z on 17/ 2/1997, from 18Z on 16/ 2/1997
LAT: 53.79 LONG: 346.97
Pressure (hPa)
600
800
100
200
300
400
Distance (km)
0.08
0.04
0
0.04
0.08

Figure 13a

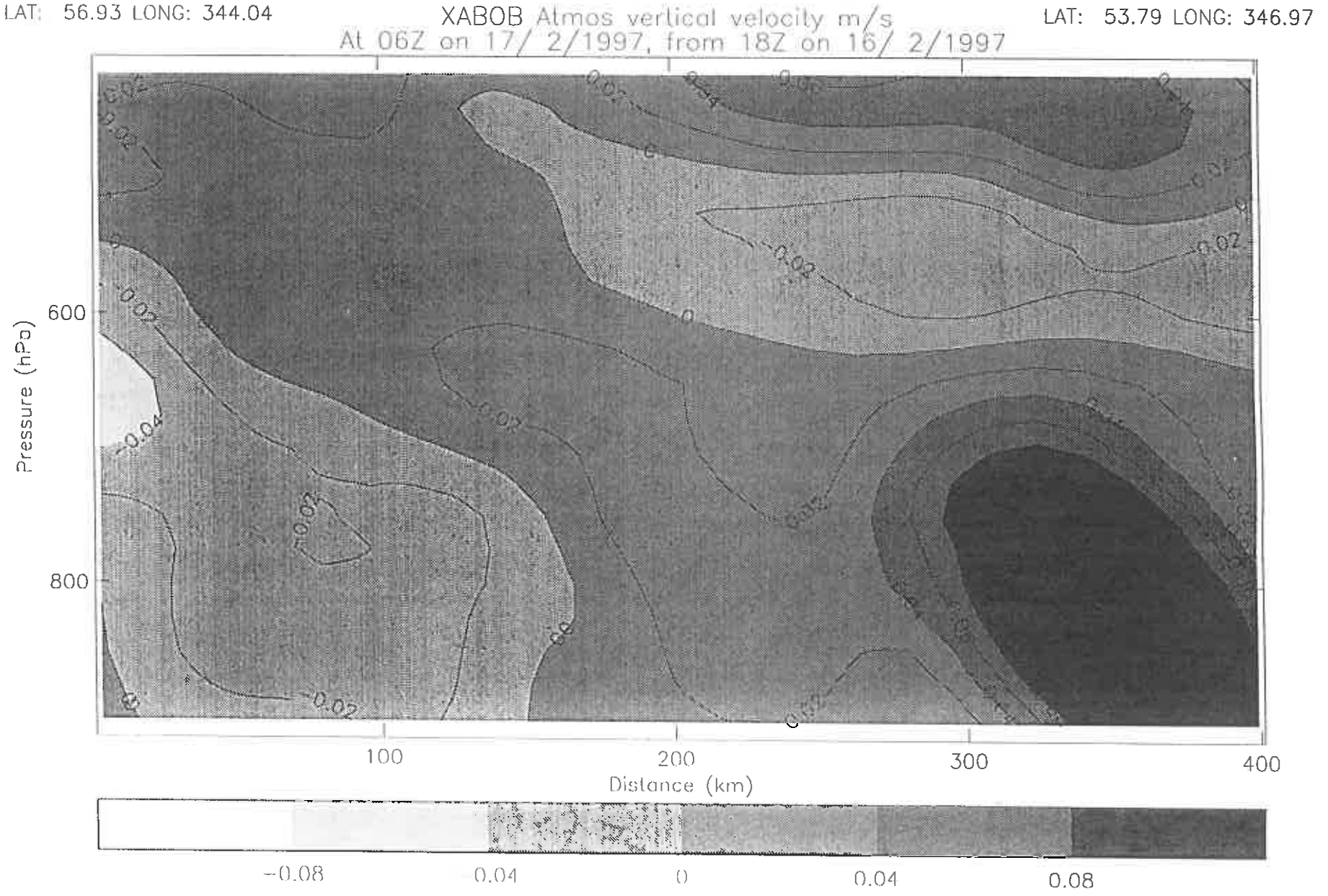
LAT: 56.93 LONG: 344.04
XABOB Atmos vertical velocity m/s
At 06Z on 17/ 2/1997, from 18Z on 16/ 2/1997
LAT: 53.79 LONG: 346.97
Pressure (hPa)
600
800
100
200
300
400
Distance (km)
-0.08
-0.04
0
0.04
0.08

Figure 13b

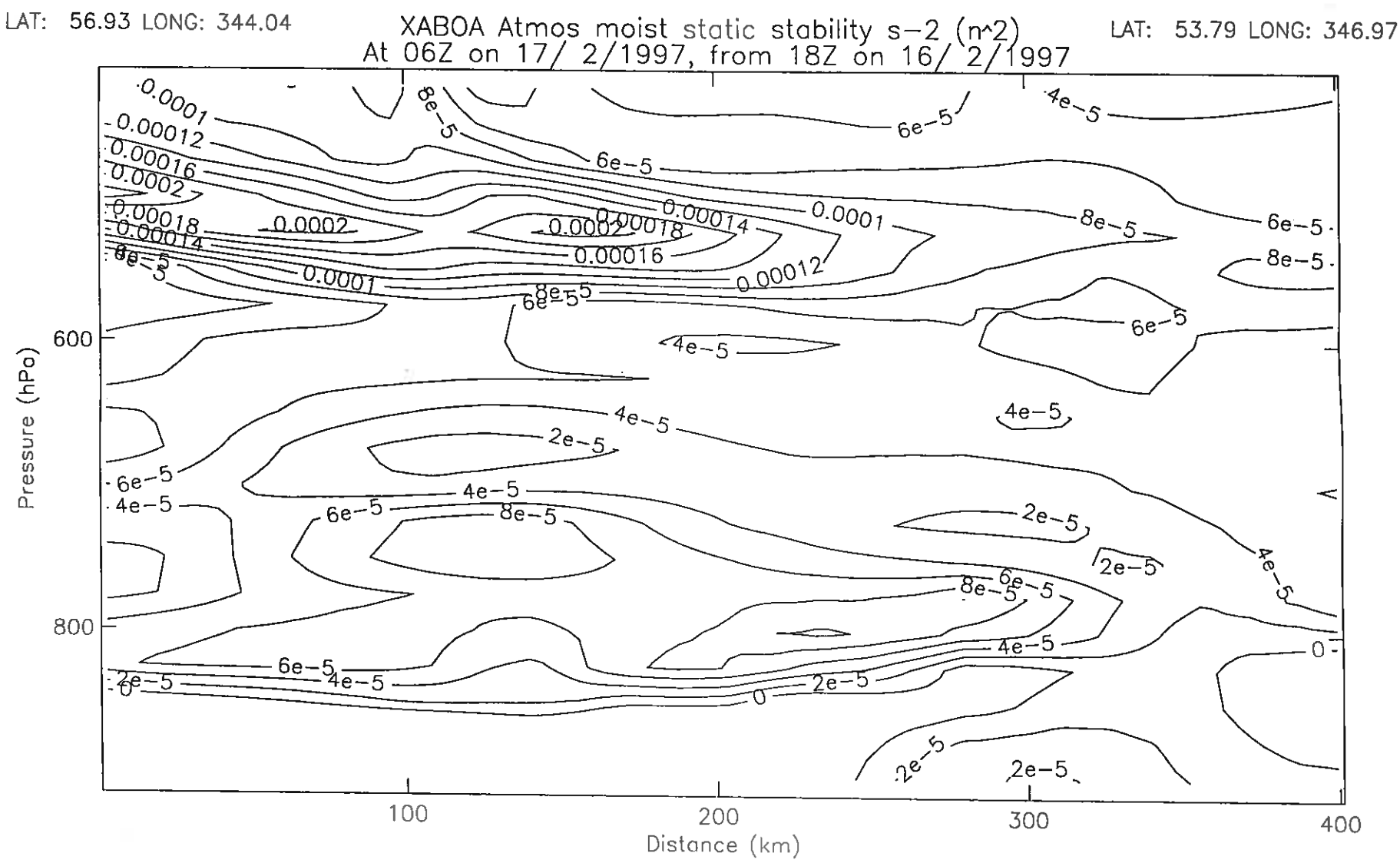
LAT: 56.93 LONG: 344.04
XABOA Atmos moist static stability s-2 (n^2)
At 06Z on 17/ 2/1997, from 18Z on 16/ 2/1997
LAT: 53.79 LONG: 346.97
Pressure (hPa)
600
800
100
200
300
400
Distance (km)

Figure 14

CURRENT JCMM INTERNAL REPORTS

This series of JCMM Internal Reports, initiated in 1993, contains unpublished reports and also versions of articles submitted for publication. The complete set of Internal Reports is available from the National Meteorological Library on loan, if required.

1. **Research strategy and programme**
   K A Browning et al
   January 1993

2. **The GEWEX Cloud System Study (GCSS)**
   GEWEX Cloud System Science Team
   January 1993

3. **Evolution of a mesoscale upper tropospheric vorticity maximum and comma cloud from a cloud-free two dimensional potential vorticity anomaly**
   K A Browning
   January 1993

4. **The global energy and water cycle**
   K A Browning
   July 1993

5. **Structure of a midlatitude cyclone before occlusion**
   K A Browning and N Roberts
   July 1993

6. **Developments in systems and tools for weather forecasting**
   K A Browning and G Szejwach
   July 1993

7. **Diagnostic study of a narrow cold frontal rainband and severe winds associated with a stratospheric intrusion**
   K A Browning and R Reynolds
   August 1993

8. **Survey of perceived priority issues in the parametrizations of cloud-related processes in GCMs**
   K A Browning
   September 1993

9. **The effect of rain on longwave radiation**
   I Dharssi
   September 1993

10. **Cloud microphysical processes - a description of the parametrization used in the large eddy model**
    H Swann
    October 1993

11. **An appreciation of the meteorological research of Ernst Kleinschmidt**
    A J Thorpe
    May 1992

12. **Potential vorticity of flow along the Alps**
    A J Thorpe, H Volkert and Dietrich Heimann
    August 1992

13. **The representation of fronts**
    A J Thorpe
    January 1993

14. **A parametrization scheme for symmetric instability: test for an idealised flow**
C S Chan and A J Thorpe
February 1993

15. **The Fronts 92 Experiment: a Quicklook Atlas**
Edited by T D Hewson
November 1993

16. **Frontal wave stability during moist deformation frontogenesis**
Part 1: Linear wave dynamics
C H Bishop and A J Thorpe
May 1993

17. **Frontal wave stability during moist deformation frontogenesis**
Part 2. The suppression of non-linear wave development
C H Bishop and A J Thorpe
May 1993

18. **Gravity waves in sheared ducts**
S Monserrat and A J Thorpe
October 1993

19. **Potential vorticity and the electrostatics analogy: quasi-geostrophic theory**
C Bishop and A J Thorpe
November 1993

20. **Recent advances in the measurement of precipitation by radar**
A J Illingworth
April 1993

21. **Micro-physique et givrage: cloud microphysics and aircraft icing**
A J Illingworth
May 1993

22. **Differential phase measurements of precipitation**
M Blackman and A J Illingworth
May 1993

23. **Estimation of effective radius of cloud particles from the radar reflectivity**
N I Fox and A J Illingworth
May 1993

24. **A simple method of Dopplerising a pulsed magnetron radar**
A Hua, A J Illingworth and J Eastment
November 1993

25. **Radiation and polar lows**
George C Craig
February 1994

26. **Collected preprints submitted to the International Symposium on the Life Cycles of Extratropical Cyclones; Bergen, Norway, 27 June - 1 July 1994**
April 1994

27. **Convective frontogenesis**
Douglas J Parker and Alan J Thorpe
April 1994

28. **Improved measurement of the ice water content in cirrus using a total water evaporator**
Philip R A Brown and Peter N Francis
April 1994

29. **Mesoscale effects of a dry intrusion within a vigorous cyclone**
K A Browning and B W Golding
April 1994

30. **GEWEX Cloud System Study, Science Plan**
May 1994

31. **Parametrization of momentum transport by convectively generated gravity waves**
R Kershaw
May 1994

32. **Mesoscale Modelling Newsletter No 5**
May 1994

33. **Observations of the mesoscale sub-structure in the cold air of a developing frontal cyclone**
K A Browning, S A Clough, C S A Davitt, N M Roberts and T D Hewson
May 1994

34. **Longwave radiative forcing of a simulated tropical squall line**
Imtiaz Dharssi
July 1994

35. **On the nature of the convective circulation at a kata-cold front**
K A Browning
September 1994

36. **Collective preprints of papers submitted to the COST-75 International Seminar on Advanced Weather Radar Systems, Brussels, 20-23 September 1994**
November 1994

37. **Use of satellite imagery to diagnose events leading to frontal thunderstorms: Parts I and II of a case study**
K A Browning and N M Roberts
November 1994

38. **The role of spaceborne millimetre-wave radar in the global monitoring of ice cloud**
P R A Brown, A J Illingworth, A J Heymsfield, G M McFarquhar, K A Browning and M Gosset
December 1994

39. **Potential vorticity inversion**
Michal Ziemianski
October 1994

40. **Theory of mature tropical cyclones; a comparison between Kleinschmidt (1951) and Emanuel (1986)**
Suzanne L Gray
December 1994

41. **Dispersion and removal of pollutants during the passage of an atmospheric frontal system**
N R Gimson
December 1994

42. **The role of snow sublimation in frontogenesis**
D J Parker and A J Thorpe
December 1994

43. **Potential vorticity and the electrostatics Analogy: Ertel-Rossby formulation**
A J Thorpe and C H Bishop
December 1994

44. **Mesoscale aspect of extratropical cyclones: an observational perspective**
K A Browning
January 1995

45. **A polar low outbreak: evolution and mesoscale structures**
T D Hewson, G C Craig and C Claud
February 1995

46. **Generation of near-surface gusts of deep convection**
K Nakamura and R Kershaw
April 1995

47. **Attribution concepts applied to the Omega Equation**
S A Clough, C S A Davitt and A J Thorpe
June 1995

48. **Parametrization of mixed-phase cloud and precipitation**
Susan P Ballard and M Gerard Hutchinson
June 1995

49. **Short-range forecasting of stratocumulus: initialization prediction**
Susan P Ballard, Simon D Jackson and B Macpherson
June 1995

50. **Contributions of the JCMM/Dept of Meteorology Radar Group to the 27th AMS Radar Meteorology Conference, Vail October 1995**
June 1995

51. **Cold pools in shear**
Douglas J Parker
September 1995

52. **High-resolution analysis of frontal fracture**
K A Browning, S P Ballard and C S A Davitt
September 1995

53. **The albedo of broken cloud fields: calculations using a modified two stream radiation code**
Imtiaz Dharssi and Roy Kershaw
October 1995

54. **Parametrization of momentum transport by convection. I: theory and cloud modelling results**
R Kershaw and D Gregory
November 1995

55. **Variation of frontal structure along a cold front**
K A Browning and N M Roberts
November 1995

56. **Secondary frontal waves**
Douglas Parker
December 1995

57. **Objective fronts**
T D Hewson
March 1996

58. **Mesoscale analysis of the activation of a cold front during cyclogenesis**
K A Browning, N M Roberts and A J Illingworth
June 1996

59. **Investigation of different representations of rain in a 1-d evaporation model**
H Swann
May 1996

60. **Parametrization of diabatic processes in the inversion of the omega-equation**
M Athanassiadou and A J Thorpe
June 1996

61. **The role of the environmental flow in the development of secondary frontal cyclones**
I A Renfrew, A J Thorpe and A Joly
June 1996

62. **Consequences of the geostrophic momentum approximation on barotropic instability**
S Malardel, A J Thorpe and A Joly
June 1996

63. **Contributions to the AMS/RMS Conference on Mesoscale Processes**
Reading, 9-13 September 1996

64. **Vorticity and potential vorticity in stratified flows interacting with an isolated obstacle**
Jorge A Gutiérrez and A J Thorpe
September 1996

65. **Triple point development: two case studies**
Douglas Parker
September 1996

66. **Radar observations of wind-shear splitting within evolving atmospheric Kelvin-Helmholtz billows**
D Chapman and K A Browning
April 1997

67. **Cold frontal structure derived from radar wind profilers**
K A Browning, D Jerrett, J Nash, T Oakley and N M Roberts
May 1997

68. **The dry intrusion and its effect on the frontal, cloud and precipitation structure of extratropical cyclones**
K A Browning - Text of invited special lecture at the Spring Conference
of the Meteorological Society of Japan, University of Tsukuba, 22 May 1997

69. **Met. Office Unified Model data, diagnostics, graphics programs, and other observational data available from the JCMM through the aegis of the Universities Weather Research Network (UWERN).** (Plus supplement)
Peter Panagi and Ed Dicks
June 1997

70. **Contributions of the JCMM/Dept of Meteorology Radar Group to the 28th AMS Radar Meteorology Conference.** Austin, Texas
September 1997

71. **Sensitivity of short-range weather forecasts to local potential vorticity modifications**
Meral Demirtas and Alan Thorpe
July 1997

72. **Objective identification of frontal wave cyclones**
T D Hewson
August 1997

73. **Attribution and its application to mesoscale structure associated with tropopause folds**
A J Thorpe
September 1997

74. **The role of the environmental flow in the development of secondary frontal cyclones**
Ian A Renfrew, Alan J Thorpe and Craig H Bishop
September 1997

75. **Potential vorticity: a short history of its definitions and uses**
Alan J Thorpe and Hans Volkert
September 1997

76. **Superposing semi-geostrophic potential vorticity anomalies**
H R Birkett and A J Thorpe
September 1997

77. **Short period forecasting of catchment-scale precipitation.**
Part 1: the role of Numerical Weather Prediction
M A Pedder, M Haile and A J Thorpe
September 1997

78. **Verification of the tracking technique used in an experimental cloud motion wind inferring system**
Z Wang, K A Browning and G A Kelly
October 1997

79. **A preliminary study of Fourier series analysis for cloud tracking with GOES high temporal resolution images**
Z Wang
October 1997

80. **Analysis of an ex-tropical cyclone after reintensifying as a warm-core extratropical cyclone**
K A Browning, G Vaughan and P Panagi
November 1997

81. **A JCMM overview of FASTEX IOPs**
S A Clough, H W Lean, N M Roberts, H Birkett, J-P Chaboureau, R Dixon, M Griffiths, T D Hewson and A Montani
January 1998

82. **Programs for PV inversion and modification**
Meral Demirtas
December 1997

83. **Release of potential shearing instability in warm frontal zones**
D Chapman and K A Browning
February 1998

84. **The European Cloud-Resolving Modelling Programme (EUCREM)**
Summary Report from the coordinator
P W White
April 1998

85. **A frontal wave database**
T D Hewson
April 1998

86. **Layering observed in dropsoundings from IOP 1 of Fronts 92**
S A Clough
May 1998

87. **Use of wind-shear displays for Doppler radar data**
D Chapman and K A Browning
May 1998

88. **Radar estimates of rainfall rates at the ground in bright band and non-bright band events**
T J Smyth and A J Illingworth
June 1998

89. **Correction for attenuation of radar reflectivity using polarisation data**
T J Smyth and A J Illingworth
June 1998

90. **The effects of convection on chemical reactions and precipitation scavenging**
Neil R Gimson
July 1998

91. **How to use the display program DISP**
Nigel Roberts
August 1998

92. **Conceptual models of cyclogenesis**
Adrian T Semple
August 1998

93. **Observations of oblate hail using dual polarisation radar and implications for hail detection schemes**
T J Smyth, T M Blackman and A J Illingworth
September 1998

94. **The semigeostrophic diagnosis of vertical motion. Part I: Formulation and co-ordinate transformations**
Mike A Pedder and Alan J Thorpe
September 1998

95. **The semigeostrophic diagnosis of vertical motion. Part II: Results for an idealised baroclinic wave life cycle**
Alan J Thorpe and Mike A Pedder
September 1998

96. **Convective destabilisation by a tropopause fold diagnosed using potential vorticity inversion**
Morwenna Griffiths, Alan Thorpe and Keith Browning
October 1998

97. **Forecast skill of the ECMWF model using targeted observations during FASTEX**
A Montani, A J Thorpe, R Buizza and P Unden
October 1998

98. **Observations and model simulations of the FASTEX IOP 16 frontal wave - effects of sublimation**
Sid A Clough, Humphrey W Lean, Nigel M Roberts and Richard M Forbes
December 1998

Met Office Joint Centre for Mesoscale Meteorology Department of Meteorology
University of Reading PO Box 243 Reading RG6 6BB United Kingdom
Tel: +44 (0)118 931 8425 Fax: +44 (0)118 931 8791
www.metoffice.com